Synthesis and Characterization of Antibacterial Bilayer Hydrogel for Wound Dressing Application

By

Shah Zeb

School of Chemical and Materials Engineering

National University of Sciences and Technology

2022

Synthesis and Characterization of Antibacterial Bilayer Hydrogel For Wound Dressing Application

Name: Shah Zeb

Reg No.: 00000320056

This thesis is submitted as partial fulfilment of the requirements for the degree of

MS in Chemical Engineering

Supervisor: Dr. Muhammad Bilal Khan Niazi

School of Chemical and Materials Engineering (SCME)

National University of Sciences and Technology (NUST)

H-12 Islamabad, Pakistan

May, 2022

Dedication

This thesis is dedicated abridgedly to my parents and siblings for their unlimited support, moral encouragement, and incalculable love.

Acknowledgements

Starting from my supervisor and co-supervisor, **Dr. Muhammad Bilal khan Niazi** and**, Dr Sulalit Bandyopadhyay** respectively. I owe them immense gratitude and respect for always believing in my, their unlimited support, guidance, and moral encouragement at unpleasant circumstances. The driving force for my untired efforts were built upon their confidence and trust in me, their consultation and precious advice helped a lot during this tedious journey. I'm extreme thankful for everything, it was honor working under their competent supervision.

I am extreme thankful to my GEC members Dr. Salik Javaid Kakar and Dr. Usman Liaqat for their directions as well.

Furthermore, I would like to express my deep feelings for my parents, no combination of words would do the justice explaining their rule in my life. Their unlimited support, encouragement, believe in me and love has inspired me to run after my goals. Their sacrifices and efforts are unpayable.

Lastly, I would express my thank to my siblings and friends for having my back in all thick and thin. Without their support and love it never would've been possible

Shah Zeb

Abstract

Nanoparticles are frequently employed in biological applications, medicine delivery, and water treatment. The concept of incorporation silver nanoparticles (AgNPs) in membranes is useful for wound dressing and covering surgical instruments because the metal base nanoparticles are the intriguing material for wound healing, antibacterial and drug carriers. A lot of study has been done in recent years on the slow release of drugs. Many researchers have tried how to accelerate the wound healing. Some authors have tried hybrid hydrogel by using different polymers to give stability and drug release properties**.** But they have not mentioned any data regarding the quantity of the drug that is released around the wound area and how much the drug should release either it releases fast or slow and which one gives the better results. Although silver has good antibacterial properties, but they have not mentioned any side effects if we increase the concentration around the wound area. They haven't mentioned the systemic toxicity of the silver because it varies in different application. We are using different sizes of AgNPs in bilayer hydrogel membrane their shape is spherical and quantity of AgNPs is constant to see its antibacterial and toxicity test for wound dressing. Silver nanoparticles was characterized by UV Vis, Zetasizer, SEM Apreo, S(T)EM, XRD and FTIR. After analyzing the AgNPs we have incorporated these AgNPs in bilayer hydrogel membrane. Bilayer hydrogel membrane was characterized by SEM Apreo, XRD, TGA, AFM. Some physical testing was also performed on membranes like swelling test, moisture retention and Water vapor transmission rate. The antibacterial activities were conducted against E. coli and the maximum inhibition zone was reported 20±5nm. MTT assay test was conducted to see cell viability % and we observe that at low concentration we get the best results between 85% to 92.2%. Future research and development would benefit from both in vivo and in vitro methods to extrapolate from and test antibiotic-loaded nanofibers in humans.

Keywords: Antibacterial; Bilayer Hydrogel; Wound Dressing

Table of Contents

List of figures

List of Tables

Abbreviations

CS = Chitosan

AuNPs = Gold nanoparticles

AgNPs = Silver Nanoparticles

NPs = Nanoparticles

$NaBH_4$ = Sodium borohydride

PVP = Polyvinylpyrrolidone

PVA = Polyvinyl alcohal

AR = Aspect ratio (Length/Diameter)

DOE = Design of Experiments

LSPR = Localized Surface Plasmon Resonance

FTIR = Fourier-Transform Infrared Spectrometry

XRD = X-Ray Diffraction

SEM Apreo = Scanning Electron Microscopy Apreo

S(T)EM = Scanning (Transmission) Electron Microscopy

TGA = Thermogravimetric Analysis

TEM = Transmission Electron Microscopy

WVTR = Water Vapour Transmission Rate

AFM = Atomic Force Microscopy

Chapter 1

Introduction

1.1 Introduction of the project

In recent years multilayer hydrogels are widely used in wound dressing because they give better healing as compared to the single layer hydrogel.[1] Multilayer hydrogel usually consists of more than two layers because they are design in such a way to fulfill the requirement for the ideal wound healing. Skin, as the largest organ in the body, is vulnerable to external attacks. Once the skin suffers serious defects, the wound will severely affect people's life and health. Wound dressing is important because it gives that optimum condition to wound so that it can heal fast. while preventing the wound from further damage and dangerous germ invasion It's also critical that the dressings be removed gently to avoid extra harm to the wound area during dressing changes. Wound healing is one of the major challenges that face by the medical science. So far, several kinds of wound dressings have been developed including rubber, foam, electro spun nanofiber, membrane, and hydrogel etc.

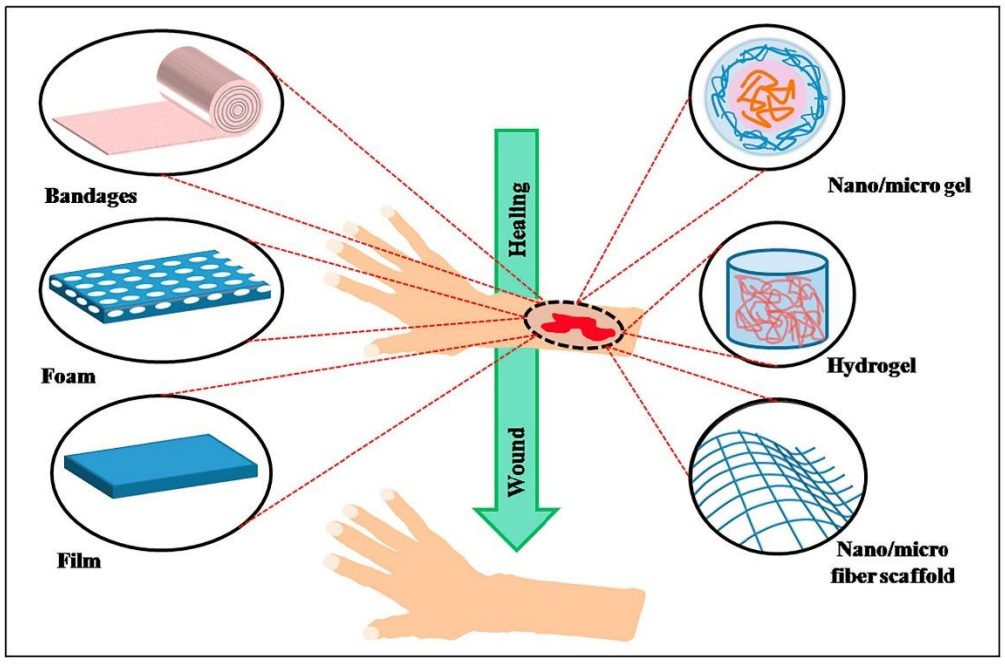

Figure 1 Several type of wound dressing [2]

Due to the complex nature of healing, issues generating sufficient preclinical models, and the expense, length, and exclusivity of trials, wound research confronts inherent barriers. These challenges can be solved with an informed approach. (1) selecting appropriate and meaningful models for preclinical trials and providing necessary information for standardization, (2) maintaining inclusion and exclusion criteria during clinical testing, and (3) developing clinical data to support the acceptance of relevant primary outcomes for wound trials beyond complete wound healing are the major steps required to improve wound research and (4) Biomarker development and personalized medicine approaches to better assess which patients are likely to respond to specific medications. These developments will enable the wound community to advance beyond the restrictions and provide real approaches to wound care improvement in the years ahead. [3] Nowadays majority of biopolymers and biomaterial are used in hydrogels. We are Focusing on multilayers layer of hydrogels so that its efficiency is increase because each layer perform their own function just like the top layer protects the moisture and other layer give support the new tissues so that the wound should recover quickly.[4]

In traditional wound dressing we face lot of problem like they are unable to protect the wound form microbial invasion. They cause lot pain to patient during removal time. They are not suitable for chronic wound; they keep the wound surface dry that cause decrease in cell proliferation. So, to solve these problems hydrogels are used as wound dressing because they have many advantages like they provide moist environment around the wound, allow oxygen to permeate, absorb wound exudates, soft in nature, antibacterial material carrier and easy to remove.

During my master project I worked on the bilayer hydrogel membranes for wound dressing applications in which the 1st layer is PVA and the 2nd layer is Chitosan. The top layer of PVA improves the mechanical properties of the membranes and control the moisture around the wound. While the second layer is of chitosan that is a bio polymer it improves the drug release properties. we are incorporating silver nanoparticles of spherical shape with different size in the bilayer membrane and see its effects on the wound dressing application.

1.2 Nanoparticles

Richard P. Feynman was the first man who presented the “nano-technology” and later got Nobel Prize. Since then, this technology has been extensively studied and used in different walks of life. He presented his work in his famous work during 1950 named “There’s Plenty of room at the bottom” [5]. After his provocation this field has revolutionized.

Nano-Technology means producing materials at nano-scales, with dimensions 100nm somewhat [6] These materials can be of zero, one, two and three dimensions [7]. Scientists revealed that particles size matters a lot, and it influences their physiological activities. Particles at this level has characteristic colors and properties subjected to their shape and size.

In recent years nanotechnology has a vital role in the numerous fields of the research. In general, the use of Metallic Nano particles (MNPs) has attract many industrial and biomedical applications due to their remarkable size dependent properties [8]. The intrinsic properties of the (MNPs) are determined by the various factors like shape, size, crystallinity, and the composition. And they all are dependent on the synthesis condition [9]. Various approaches have been used for the synthesis of MNPs such as photochemical approach, physical, chemical, and biological.

1.2.1 Classification of Nanoparticles

Nanoparticles are divided on the base of size, chemical properties, and the morphology

1.2.1.1 Carbon base NPs

The main particles that of this class are fullerenes and carbon nano=tubes (CNTs). The Globular hollow cage nano material is called fullerenes. Fullerenes are the allotropic form of the carbon. Due to their excellent properties these have fetched the commercial interest such as high tensile strength, electron negativity and electric conductivity.[10]

Carbon nano tubes are elongated and size of 1-2 nm. Graphene sheet rolling upon it well predicts their structure. These sheets can be found in single, double, or multiwall wrapped structure that why they can be named as single-walled nanotubes, on the other side double walled nano tubes are multiwalled nanotubes. Commercial application of these is used in their pristine form along with nanocomposite [11]**.**

1.2.1.2 Metal NPs

Metallic nanoparticles are purely formed by their metal precursor. These particles exhibit optoelectrical property in the broad solar spectrum Au, Ag and Cu NPs Absorption band lies in the visible zone. Due to these important properties of the nanoparticles, they have many industrial applications and in research area like Gold NPs are widely used for the enhancement of the sample of electronic steam hence producing high quality SEM images [12]**.**

1.2.1.3 Ceramic NPs

Ceramic NPs are Nonmetallic and inorganic in nature, ceramic particles are produced by using heating and cooling. These particles are found in different forms such as polycrystalline, amorphous, porous, and hollow forms. These NPs are used in many dire fields like catalysis and make them imported class of chemicals. They are also used in photocatalysis imaging application and photo degeneration [13]**.**

1.2.1.4 Polymeric NPs

Polymer nanoparticles are called polymeric nanoparticles in common literature, and they are usually found in the nanospheres or nano capsular shapes. Nanospheres are matrix particles with certain mass that is solid in general these molecules are absorbed outside the surface of the polymer. While the nano capsules the complete solid mass is encapsulated in the particle because these particles have the ability to functionalized in the variety of application [14, 15]**.**

1.2.2 Nanoparticle Synthesis

There exist numerous ways to synthesize NPs and the methods can be classified as either a "top down" or "bottom up" approach. In the top-down procedures, the NPs are derived from larger molecules, whereas in the bottom-up approach they are synthesized by nucleation and growth of molecular distributions in either liquid or vapor phase. Bottom-up procedures are the most often utilized ways for synthesizing NPs because they allow for a more regulated synthesis in terms of particle shape and size. Generally, for a bottom-up synthesis of NPs to take place, three components are required: a precursor, reducing agent and surfactant. The precursor provides the material of which the NPs will compose, the reducing agent reduces the precursor into the atoms serving as building blocks for the

NPs, and the surfactant stabilizes the synthesized NPs by preventing aggregation and other unwanted phenomena such as Ostwald ripening[16, 17]

1.2.3 Antimicrobial NPs

Antimicrobial activity in the nanoparticles is used to slow down the growth or killing of bacteria, without giving any toxic effect to the environmental. The antimicrobial agents are usually used to modify the chemical compound, furthermore these agents are classified into two more groups one is bactericidal and second one is bacteriostatic these both are used to slow down the growth of bacteria and kill the bacteria.[18, 19]

This antimicrobial agent has Hight capacity to fight against the bacteria because they are widely used, and they abuse the new bacteria with resistant properties. These antimicrobial agents cause the bacterial change in the micro evolution against the persistent.[20]

World health sector act against the antimicrobial agent due to their high risk and infection diseases. Due to these types of issues now nanomaterials are emerged as novel agent against the bacteria that kill the bacteria and slow down the growth. These nano size materials are effectively treating the diseases[21].

Nanomaterials' remarkable antibacterial capabilities are due to their high surface to volume ratio, which boosts their chemical, physical, magnetic, and magneto-electrical properties, which are considerably different from their parent chemicals. So, in this bacteria-fighting scenario, nanoparticles are shown to be fascinating materials[22].

1.2.4 Working mechanism of NPs against Bacteria

Recent study on nanoparticles and bacteria has revealed that the specific method by which these nanoparticles work against bacteria is yet unknown. However, some hypothesized methods suggest that nanoparticles can be connected to bacterium membranes by compromising membrane integrity via electrostatic contact. Free radicals produced because of oxidative stress, causing nano-toxicity, and killing microorganisms. The harmful action of various anti-bacterial NPs towards bacteria is depicted in the diagram below [21].

1.3 Silver Nanoparticles

Recent study on nanoparticles and bacteria has revealed that the specific method by which these nanoparticles work against bacteria is yet unknown. However, some hypothesized methods suggest that nanoparticles can be connected to bacterium membranes by compromising membrane integrity via electrostatic contact. Free radicals produced because of oxidative stress, causing nano-toxicity, and killing microorganisms. The harmful action of various anti-bacterial NPs towards bacteria is depicted in the diagram below[23].Silver nanoparticles has been used in diverse range of materials owning to their wonderful properties, such as application is consumer products, medical, agriculture and food. Silver-based nanomaterials have been employed in the wound healing industry since the 1970s. During this time, the usage of these particles in wound management increased over the world.

Silver (Ag^{+}) generally is an inert element, but when it encounters with wet environment, it produces ions that are thought to have antimicrobial and antibacterial properties. The steps involved in bacterial demise are as follows: first, Ag+ penetrates the cell wall, breaks DNA, and hence slows cell reproduction. Different studies have proven the non-toxicity nature of silver-nano particles, such as Rigo and co-worker has conducted in vitro and in vivo studies of AgNPs, and results indicated the absence of toxicity. Keeping the valuable properties of these nano-particles materials, we have chosen them for wound healing.[24]

1.3.1 Approaches for Preparation of Silver nanoparticles

1.3.1.1 Photochemical Approach

In photochemical approach photo reduction method is used to synthesize the MNPs. By using the photoreduction approach various properties are obtained in the end constant size, absolute diameter and the distribution ratio of the particles are average and highly advance instruments are used that are quite expensive and the duration of the experiment time is long.[25]

1.3.1.2 Physical Approach

MNPs are also synthesized by the physical approaches the methods that are used in physical approaches are laser ablation, ball milling and the chemical etching methods are widely used in this approach. The advantages of the physical approaches are their speed

and less use of the chemicals but it has some drawbacks high energy is required in this process and the distribution of the particles is wide and it has low yield.[26] This approach gives pure solution of colloids and high fabrication quantity in the end, but it has some requirements huge amount of atmospheric pressure and expensive instruments.[27]

1.3.1.3 Chemical Approach

MNPs are synthesized by using this approach and the methos that are used in this approach are chemical reduction, Son chemical and electrochemical methods are used in this approach. This is efficient and simple approach its operational cost is low and mostly spherical shape are obtained in the end. The requirement for this approach is metal precursors, reducing agent and the stabilizing/capping agent.[28]

1.3.1.4 Biological Approach

The methods that are used in the biological approach are algae mediates, plant medicated and fungi & Bacterial medicated methods. This approach is environmentally friendly, but it has come complex operation, but its overall cost is low and the requirement for this approach is algae, reducing agent, fungi, non-pathogenic and bacterium. [29]

Table 1. Properties, application, and size of various nanoparticles

Nano systems	Properties	Application	Size (nm)
Metallic nanoparticles	Smaller size and stability	Drug delivery and radiotherapy treatment	< 100
Polymeric nanoparticles	Biocompatible and biodegradable	Drug carrier	10-1000
Carbon nanotubes	Electrical properties and allotropic crystalline form	Enhance solubility act as genre carrier act as peptide carrier	Diameter 0.5-3 and length 20-1000
Dendrimers	Highly branched monodispersed characters	Control delivery of bioactive and long circulatory	< 10

1.4.1 Optical and plasmonic Properties

Silver (Ag), gold (Au), Platinum (Pt), and other noble metals are commonly used in plasmonic nanoparticles. They are also valued for their exceptional qualities. Because metals have highly mobile surface electrons, they exhibit a distinct localized surface plasmonic resonance (LSPR). Light waves cause the LSPR phenomenon, and these waves are confined within metallic NPs that are typically smaller than the wavelength of the

light[30] When light interacts with matter, it causes a simultaneous oscillation of free electrons in NPs that are present in the resonance of the incident light's electric field.[31]

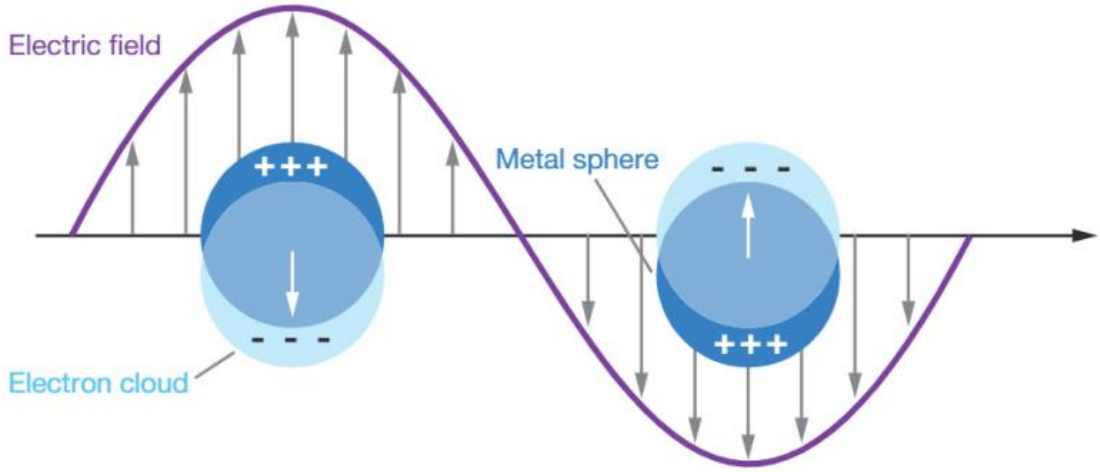

Figure 2 Schematic illustration of localized surface plasmonic resonance (LSPR)[32]

LSPR of metallic NPs has high electrical field near the surface of the metal and due to this it gives high absorption and scattering properties that are used in the various application like photothermal therapy. Plasmonic NPs are employed in this therapy to deliver in the cancer tumor and are irradiated by laser light that is absorbed by the particles.[33, 34]

The light that is absorbed is non-radiatively eased and this result give the thermal energy that are released that kills the diseased tissue. The wavelength at which the LSPR occur is usually depends upon following factors like size, geometry. Composition, particles to particles distance of NPs and dielectric environment. Plasmonic NPs of varied shapes and sizes are utilized to modify the optical characteristics of the material in various ways. [35, 36] . The size of Nanoparticles also determines the incoming light that will absorb or scattered. For the smaller size nanoparticles range up to 20 nm, because the absorption is a predominant process that will increase the dimension of effective size of nanoparticles will increase the probability of the scattered light.[30]

1.4 General Nucleation and Growth theory

In a crystal state, the crystallization process is the phase shift of a substance from a high free energy state to a low free energy state. The crystal state is defined by a recurring pattern in which crystal structures are grouped in a linear configuration. The process of formation of crystals is divided into 2 steps one is nucleation and the other one is growth. Nucleation is the first stage in the development of a new phase or the birth of a solid [37] It can site on additional monomeric building blocks and deposit in the second step, which is growth, after the first nucleus is formed[38]

LaMer model is used to describe the mechanism of nanoparticles formation through nucleation and growth that is describe in the figure below. In short nucleation, is a thermodynamic model that show the appearance of the new phase called nucleus. It is the metastable phase or primary phase. The classical nucleation theory describes that the main phenomena behind the thermodynamic fact that minimize the Gibbs free energy. There are two types of nucleation one is homogeneous nucleation and the second is heterogeneous. In homogeneous nucleation the reaction is spontaneous that require the super critical state such as supersaturation. while in heterogeneous nucleation the nucleation occurs on the solid surfaces [39]

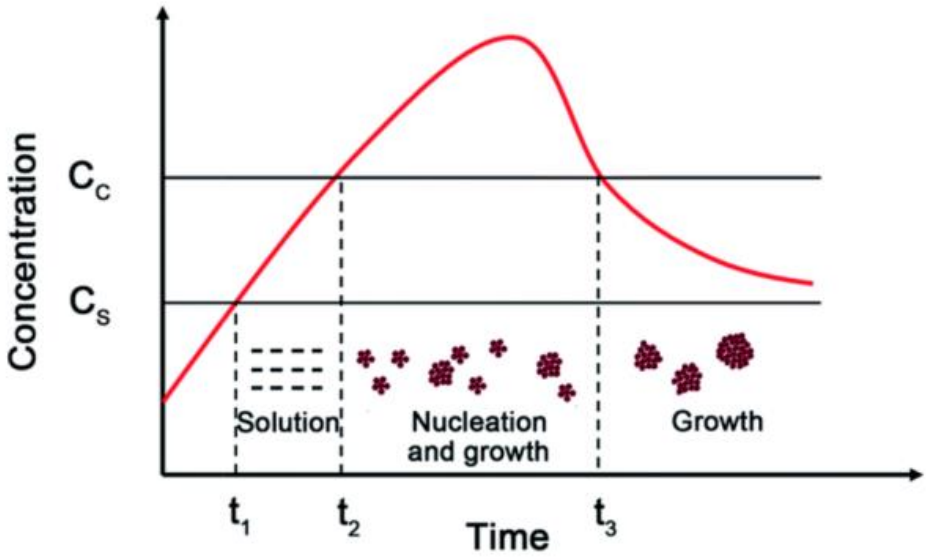

Figure 3 LaMer diagram description general nucleation and growth [40]

In the LaMer diagram, the red curve shows that the concentration of theoretical monomer in the solution as a function of time. Initially the monomers concentration is increased (usually due to reduction in case of metallic NPs).

At t_1 the critical supersaturation level (CS) is reached, and homogeneous nucleation is possible, but effectively infinite. At t_2 the saturation reaches a level (CC) at which the energy barrier for nucleation can be overcome, leading to a rapid self-nucleation. This rapid nucleation causes the supersaturation level to lower to below CC (at t_3), ending the nucleation period. Then, Diffusion of additional monomers in solution to particle surfaces causes growth. Heterogeneous nucleation/growth can be regarded as this growth[41].

Chapter 2

Literature review

2.1 Information about hydrogel

Hydrogels are three-dimensional polymeric networks that are either physically or chemically cross-linked and have hydrophilic characteristics. Hydrogels have been employed in a variety of engineering disciplines due to their various features, including great swelling, softness, and the ability to mimic natural tissues. Tissue engineering, fat, muscle, blood vessels, wastewater treatment, agriculture, medicines, sealing, biosensors, contact lenses, and food additives are all applications for these. Hydrogels are great materials for wound healing because of their outstanding moisture retention characteristics. Moisture exudates absorb in the hydrogel, preventing a foul odor from developing later.

2.2 Wound Dressing

Wound dressings cover wounds and protect the inner skin from external infections, as well as assisting the body in the formation of new skin cells that can host tissues and aid in the wound healing process.[42] There are four essential requirements for an excellent wound dressing. (1) It can keep moisture in the wound region and help the wound exude while it heals. (2) It has a suitable surface with biochemical properties that encourage cell attachment and growth. (3) It is compatible and does not have any toxic or inflammatory effects. (4) It has strong mechanical and physical properties that prevent the material from breaking and microorganisms from infiltrating it[43]. Hydrogels, semipermeable membranes, semipermeable foams, hydrocolloids, and nanogels have all been produced and employed in wound dressing in recent years to enhance wound healing.[44] However, because to their 3D porous structure, superior hydrophilicity and biocompatibility, and extracellular matrix, hydrogel is the most suited candidate in the wound dressing market.[45]

2.3 Characteristics of ideal wound dressing

2.3.1 Non toxicity

The most crucial feature of any dressing for wound healing is that it is non-toxic in nature. Toxicity in any amount may lead to unwanted consequences.

2.3.2 Bacterial infection prevention

Bacterial infections not only delayed the healing process, but also slowed it down. Bacterial infection must be avoided for rapid healing and pain alleviation.

2.3.3 Moisture

Cell proliferates in moist environments; hence moist wounds are required circumstance for wound healing. Optimum moisture level must be maintained by any wound healing dressing to help healing process.

2.3.4 Thermal insulation

Thermal insulation keeps the wound surface at the right temperature for rapid healing and pain relief. As a result, wound dressing materials should be thermally insulators.

2.3.5 Oxygen permeation

Because oxygen boosts cell activity, wound dressings must be breathable to allow oxygen to spread and promote wound healing.

2.3.6 Cost Effective

Aside from other factors, pricing is an important consideration. As a result, cost-effective wound dressings are always chosen over expensive wound dressings. A good wound dressing should be affordable.

2.3.7 Easy availability

Another key issue is the flexibility of wound dressing may be obtained by all health centers and patients. It is predicted that ideal dressings will be readily available.

2.3.8 Physical and Mechanical properties

Wound dressings must be strong enough to mimic natural skin mechanically. Chitosan has been widely used in wound dressing applications due to its unique qualities that promote wound dressings, such as biocompatibility, immune stimulatory, and low toxicity. Chitosan is ideally suited to the function of wound healing and has beneficial effects on wounds due to the qualities listed above. Various investigations have

demonstrated that chitosan is cyto compatible, however it is vulnerable to organic and inorganic pollutants and impurities due to its natural nature.

2.4 Stages of Wound Dressing

The wound repair is generally divided into four coordinated processes that are hemostasis, inflammation, proliferation, and remodeling[46]. Furthermore, wound healing may not always occur in the same order as it should since there are several factors that might induce abnormalities in wound healing, such as excessive inflammation or accidental skin damage in which tissues of skin are loss, burns[47], infection and others [8].

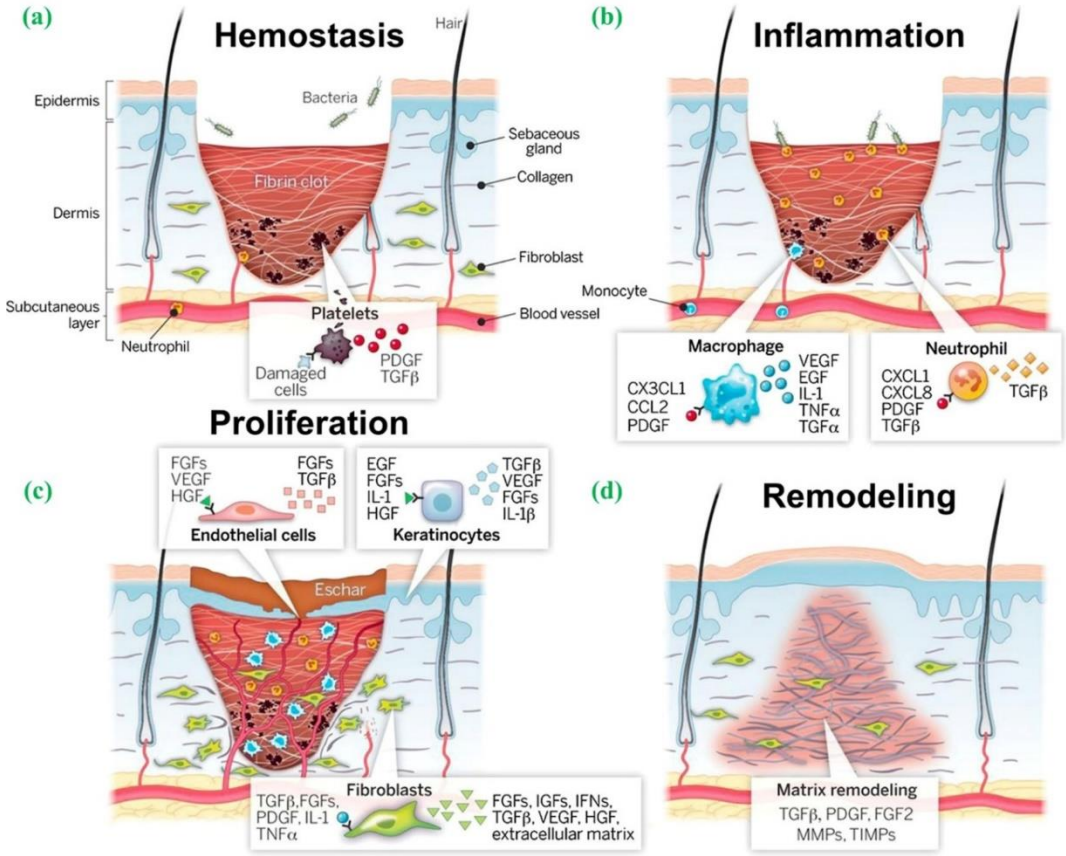

Figure 4 Stages of wound healing [48]

2.4.1 Nanomaterial based Wound dressing

Wound dressing is a painful process because it is manually adhered to the wound's surface, and it is not a comfortable substance because the material for wound dressing can only be produced by wound dehydration, which is a replacement for wound dressing.[49, 50]. Due

to this wound healing therapy that based on the utilization of Nano materials has provided and this new approach give better result and benefit. Because nanomaterials are utilized as carriers for delivering medications, and the majority of nanomaterials are based on their physicochemical qualities, nanomaterials have the ability to heal wounds due to their extraordinary nanoscale features. [51, 52]. Nanomaterials have three important characteristics that aid in wound healing: they are biocompatible and biodegradable, they have surface charge, and their colloidal stability is influenced by their size and functionalization. Furthermore, when nanoparticles are employed as active components, the wound healing process can be improved.[51, 53]

2.4.2 Skin and Nanotechnology

The skin is an important element of the body that serves as a physical, biological, and chemical barrier. It aids and protects the body from external pathogens and guards against the loss of excess fluid since it is the body's first line of defense against the external environment.[54] When the outer layer of the skin is damaged and does not heal properly, it can lead to a variety of skin problems such as irritation and bacterial infection. As a result, excess fluid is lost, and your immune system is disrupted because your body protein is lost, affecting your health, and potentially threatening your life. As a result, it is vital to repair the skin's integrity so that hemostasis can be completed on time.[55] Nanotechnology has a significant impact in the fields of medicine and drug delivery, and it is also used in subfields such as diagnosis and tissue engineering. Nanotechnology's main advantage is that it allows for rapid recovery, and most of its area is covered by skin and tissue engineering. Furthermore, when nanosized material is mixed in a polymeric structure, its performance is increased to an exceptional level. Because of these properties, nanotechnology is used in conjunction with new technologies to create and utilize surfaces, materials, and other nanotechnology-related devices at the molecular level.[56]

Chapter 3

Materials and Methods

3.1 Chemicals

Polyvinyl alcohol (PVA), chitosan (CS molecular weight 6 lacs to 8 lacs), Acetic Acid (2% w/w), Sodium Borohydride (NaBH4), Hydrazine hydrated (80 % solution in water), Iso ascorbic Acid (98 % $C_6H_8O_6$), Silver nitrate (AgNO3) and Polyvinylpyrrolidone (PVP molecular weight 10000) is purchase from Sigma-Aldrich.

3.2 Synthesis of Silver Nanoparticles

3.2.1 Synthesis of Silver nanoparticles with Sodium Borohydride.

For the synthesis of silver nanoparticles by using sodium borohydride I prepared 10 ml PVP solution of 0.375 mM and 10 ml solution of AgNO3 with 0.02 M vigorously stirring at room temperature for 5 minutes. After mixing add drop by drop 10 ml solution of NaBH4 with 0.01 M by using the pump. After adding all the solution of NaBH4 drop by drop. The mixture was continuously stirred for 10 min. and then red solution is obtained. After that centrifuge the complete solution at 14000 RPM for 3 time and wash with MQ water and disperse the Nanoparticle solution in 5ml of MQ water and store in a glass vail and cover the vail with aluminum foil.

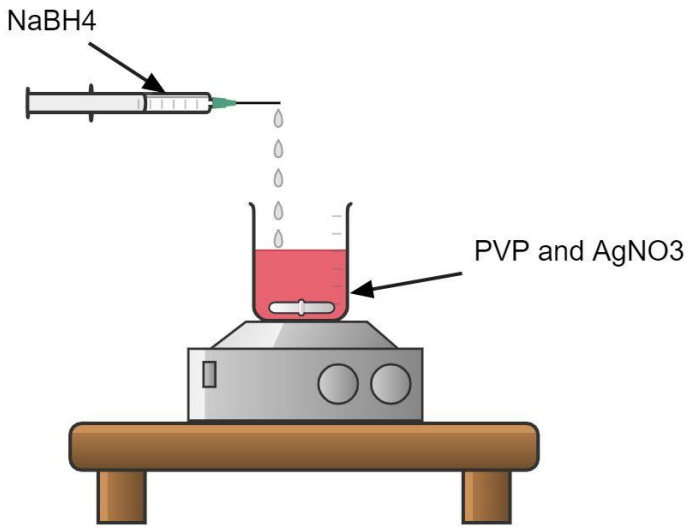

Figure 5 Synthesis of AgNPs when Sodium Borohydride is used as Reducing agent

3.2.2 Synthesis of Silver nanoparticles with Hydrazine.

Same method is followed, but the reducing agent is different N2H4. H2O. After mixing PVP and AgNO3 for 10 min. Add drop by drop solution of Hydrazine after adding stirrer it for 10 minutes and then green solution is obtained. After that centrifuge the complete solution at 14000 RPM for 3 time and wash with MQ water and disperse the Nanoparticle solution in 5ml of MQ water and store in a glass vail and cover the vail with aluminum foil.

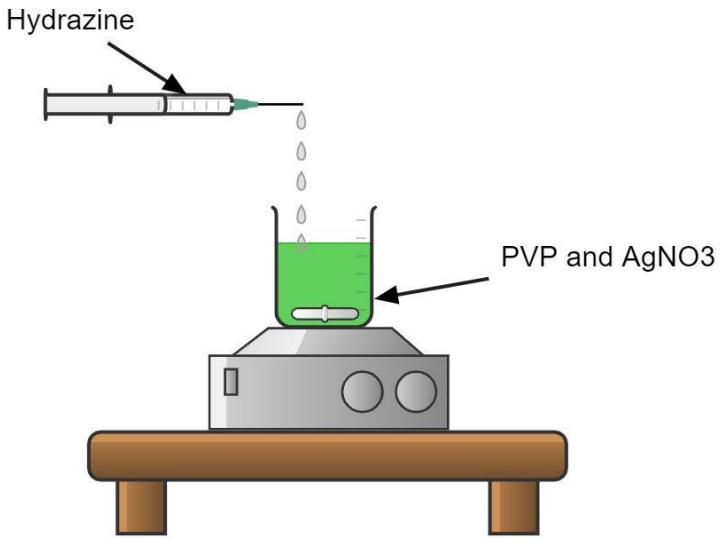

Figure 6 Synthesis of AgNPs when Hydrazine is used as reducing agent

3.2.3 Synthesis of Silver nanoparticles with Ascorbic Acid.

Same method is followed, but the reducing agent is different Ascorbic acid. After mixing PVP and AgNO3 for 10 min. Add drop by drop solution of Ascorbic acid. Stirrer the solution for 10 minutes and then light-yellow solution is obtained. After that centrifuge the complete solution at 14000 RPM for 3 time and wash with MQ water and disperse the Nanoparticle solution in 5ml of MQ water and store in a glass vail and cover the vail with aluminum foil.

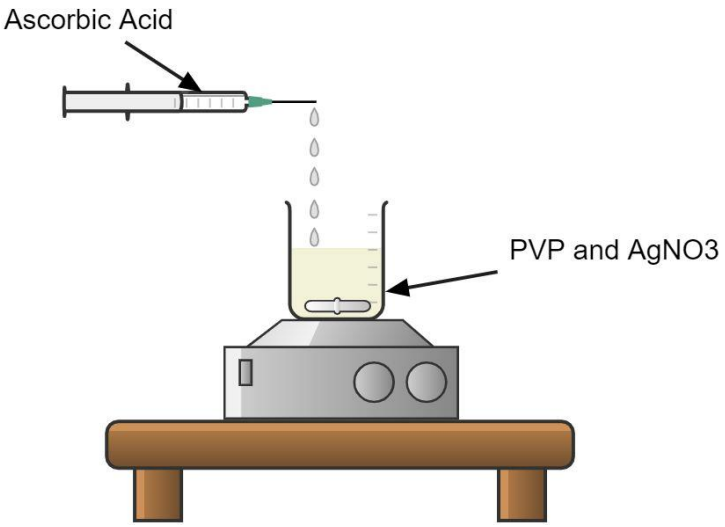

Figure 7 Synthesis of AgNPs when Ascorbic acid is used as Reducing agent

3.2.4 Seeded growth Synthesis of Silver nanoparticles

Same method is followed to synthesize the silver nanoparticles (AgNPs) of bigger size. We use the same protocol in which we add 250ul seed of Sodium Borohydride after mixing PVP and AgNO3 for 10 min. Add then we add the reducing agent drop by drop solution of sodium borohydride. After that we stirrer the solution for 10 minutes and then reddish solution is obtained. After that centrifuge the complete solution at 14000 RPM for 3 time and wash with MQ water and disperse the Nanoparticle solution in 5ml of MQ water and store in a glass vail and cover the vail with aluminum foil.

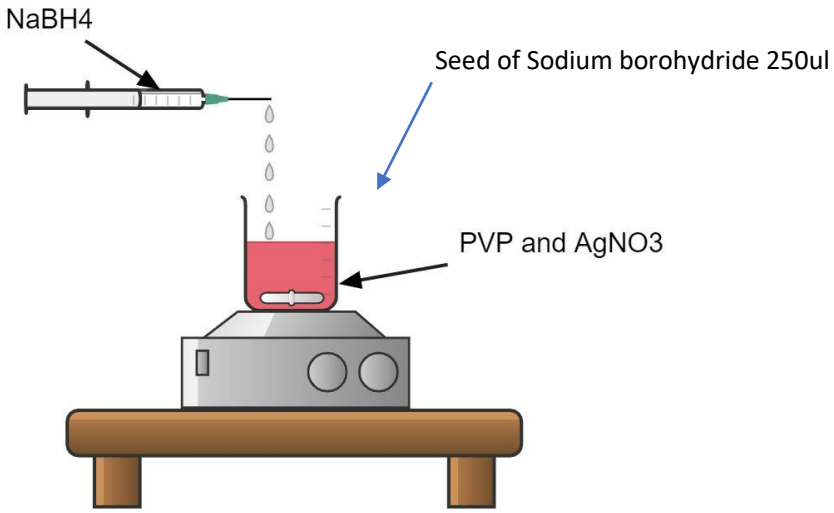

Figure 8 Seeded growth synthesis of silver nanoparticles

3.3 Design of Experiment

After completing chemical synthesis using three different reducing agents, we notice that the size and shape of the particles change when the reducing agent is changed. So, to see the difference, we used JMP software and created a screening design in which we changed different parameters like flow rate, PVP concentration, AgNO3 concentration, and reducing agent. To check at which condition we were getting the right size and shape. To fit the multivariate linear model to data set to see the selection of variables that we use in our design. The effect of the various parameter on variation of the response were analyzed by checking the R2 values the model that we fit. The least important covariates were not considered in each successive run so that we can get the response parameter that has significant impact on variability of response parameter.

Table 2. Parameters of Design of Experiment

Parameters			
Flowrate	0.05 ml/min	0.2 ml/min	0.6 ml/min
Concentration of PVP	0.187 mM	0.375 mM	0.75 mM
Concentration of AgNO3	0.01 M	0.02 M	0.03 M
Type of reducing agent	Sodium borohydride	Hydrazine	Ascorbic Acid

3.4 Synthesis of Bilayer Hydrogel membrane

For bilayer syntheses, we used 20% w/v PVA dissolved in MQ water and heated for 3 hours at 75°C until a homogeneous mixture was formed. After cooling the solution, cast the first layer on a petri dish and place it in a fume hood for 24 hours. When the first layer is semi-dry, pour the second layer of chitosan onto the petri dish. For chitosan synthesis, we used 0.5g of chitosan and dissolved it in 20ml of 2% acetic acid until a homogenous mixture was obtained.

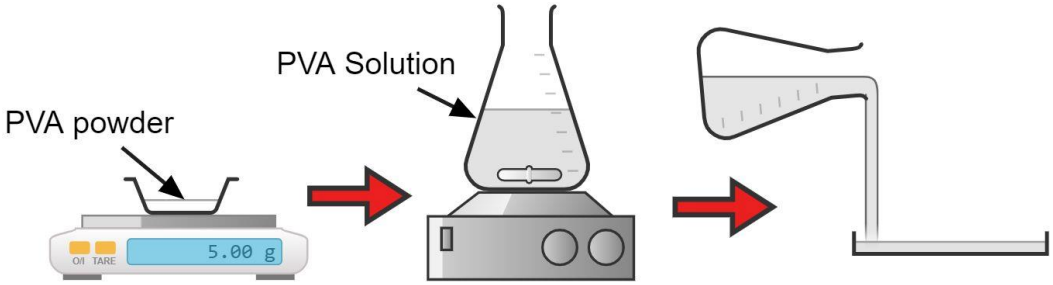

Figure 9 Casting of 1st layer of PVA

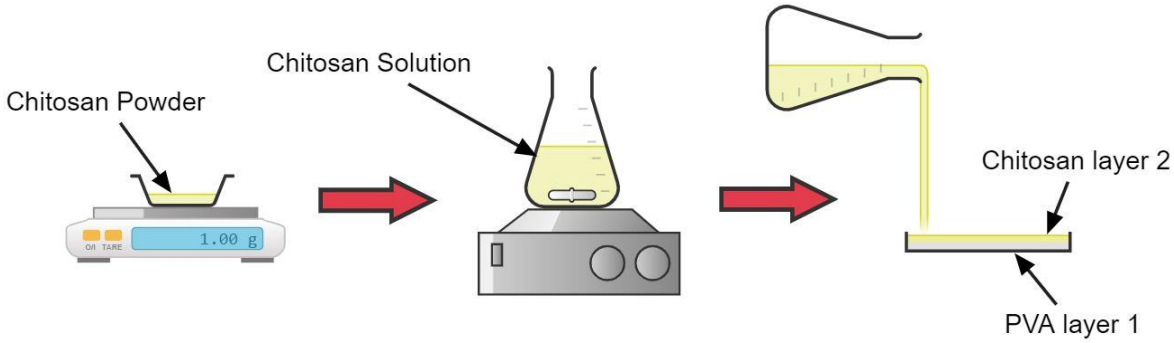

Figure 10 Casting of Bilayer hydrogel membrane

Chapter 4

Characterization Techniques

4.1 UV-VIS (Agilent Cary 60)

The UV-Vis spectroscopy is a quantitative method that measure the intensity of the light that is absorbed by the chemical specie. The measurement of the UV-Vis is based on the comparison between the intensity of the light that passed through a sample with the reference sample or the blank sample. The reference sample or blank sample is usually solvent medium which the chemical dissolved. By using the UV-Vis spectroscopy we can quantify the amount of concentration of the known sample by studying the number of photons that reach the detector. The concentration of the sample is directly related to intensity of the light that is absorb at specific wavelength.

Figure 11 UV-Vis (Agilent Cary 60)

4.1.1 Working Principle of Agilent Cary 60

As the light is absorbed the matter, there is the increase in the energy content of the atom or molecules. When the ultraviolent light is absorbed, the electron is excited from the ground state toward a higher energy state. The molecules containing π electron or non-bonding electron that can absorb energy in the form of ultraviolent light to excite these electrons to higher anti-bonding molecular orbitals. The excited electron has longer wavelength of the light because they can absorb more. Absorption of the ultraviolent light

by chemical compound produce a distinct spectrum that helps in the identification of the compound.

4.2 Lite Sizer

When we are dealing with nanoparticles the size and the stability of the nano and macro particles play avital role depend upon their performance and their functions. Lite sizer 500 is used to measure the size of particle, zeta potential and the molecular mass by using dynamic light scattering technology. Lite sizer 500 uses simple software by using the three-detection angle like side, back and forward scattering. these angles allow for the optimal parameter settings. This will also include automatic angle selection; the lite sizer automatically defines the most appropriate angel that fit on your sample. Lite sizer 500 also use backscatter angle that is ideal for turbid sample because it can reduce the multiple scattering and give a quick result with optimal data quality.

Figure 12 Lite Sizer 500

4.2.1 Working Principle of Lite Sizer 500

The laser illuminates on the sample that is inside the cell. The laser light is scattered by the particles that in the sample and the intensity of the light that is scattered by the particle is measured by some detector. The range of the scattered light must be in the specific range and to reduce the intensity an attenuator is used. The scattered particles produce some signal that passed through a detector and convert into digital by the processing board called correlator. The correlator compares the intensity of the scattered particle at successive time interval to drive the rate at which the intensity is changing. The information that is obtained from the correlator is passed to zetasizer software where the size information of the particle is analyzed

4.3 Zeta View (Particle Tracking Analyzer)

ZetaView is the instrument used for nanoparticle tracking analysis it is used for measuring the hydrodynamic particle size, zeta potential and concentration of the particle. By using nanoparticle tracking analysis, you measure what you see because each individual particle in the field of view is counted and tracked in the short video clip, by creating the accurate concentration calculations and distribution of the particles. Zetaview combine the measurement with classical micro-electrophoresis, for the zeta-potential determination all the parameters can be measured in both scattering mode as well as in fluorescence mode, for determination of fluorescently labelled sub populations. In the result zetaview is a compact instrument for measuring size, concentration, zeta potential and fluorescence.

Figure 13 ZetaView (particle tracking analyzer)

4.3.1 Working Principle of Zeta View

Particle that are present in the sample are visualized by the illumination with a laser beam. The scattered light of the particles is recorded with the light sensitive CCD or CMOS camera that is arranged at 90^{o} angle to irradiate the plane. The 90^{o} arrangement is also known as ultra-microscopy allows detection and tracking of the Brownian motion of 10 to 1000nm sized vesicles. By using the special algorithm, particles are detected, and their path is registered. The movement of the particle per time interval is recorded and quantified as the mean square displacement. Depend on the number of dimension (one, two or all three dimensions) the observed mean square displacement, diffusion coefficient, can be calculated by using the formula below.

$$d = 16\ k_B T / 3\pi\eta(x,y)^2$$

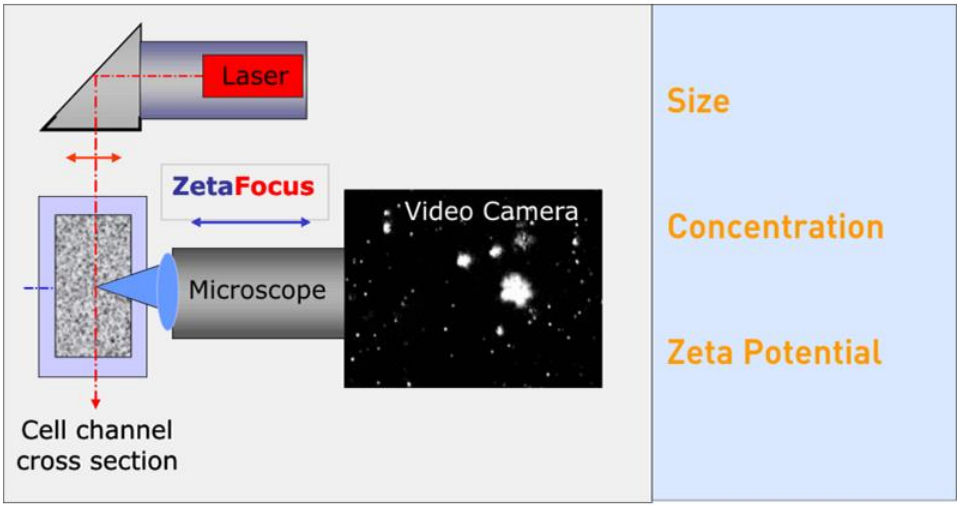

Figure 14 Working Principle of ZetaView

4.4 SEM Apreo

The SEM Apreo was used to examine the morphology of silver nanoparticles and hydrogel membranes. The silicon wafer was cleaned in a plasma cleaner prior to analysis to remove contaminants from the sample and wafer. SEM Apreo has four detectors ETD (in chamber), T1 BSE (in lens), T2 SE (in lens) and Directional Backscattered Detectors (DBS lens mounted) it has 3 operational lens modes Standard, optiplan and immersion mode. In SEM apreo, the achievable resolution is 1nm @ 1 kV, depending on the material. The highest beam current is 400 nA and the acceleration voltage is 0.2-30 kV. It also has chamber navigation camera and chamber camera CCD. SEM apreo is very elaborate and user- friendly system.

Figure 15 SEM Apreo

4.4.1 Working Principle of SEM Apreo

First, we must vent the chamber and check whether your sample is magnetic. After that load your sample on the stage holder. And evacuate/pump the chamber after that turn on the electron beam and move the region of interest, after finding the clear focus on the sample we must link the Z-position to free working distance (FWD), find the eucentric height if needed. Then start doing the high-performance imaging.

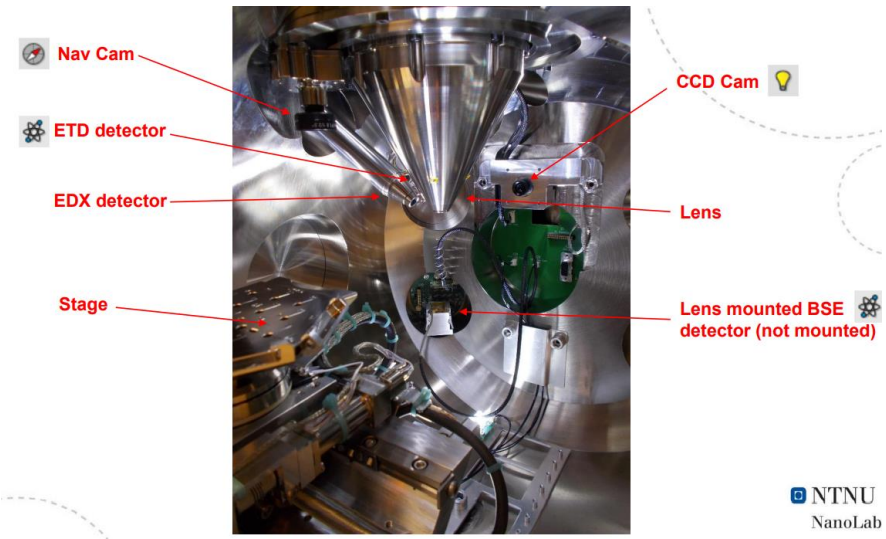

Figure 16 SEM Apreo main chamber

4.5 STEM

S(T)EM (scanning (transmission) electron microscopy) is a technique that combines the capabilities of scanning electron microscopy (SEM) and transmission electron microscopy (TEM) (TEM). A high energy focused beam of electrons is pointed towards a thin sample, and the electrons are scattered or transmitted depending on the sample's interactions. The electrons are subsequently caught by detectors, which are used to create

Figure 17 S(T)EM (scanning (transmission) electron microscopy) Hitachi High-Tech SU9000 S(T)EM (NTNU Nano Lab

a virtual image.[32]

To prepare S(T)EM samples, we use a protocol in which we place multiple drops of the sample depending on the concentration if your concentration of nanoparticles is high then you must dilute your sample. The minimum sample that we use is (60-100 µl) on a formvar carbon coated copper grid. I get the S(T)EM grid form a PhD student; S(T)EM trainings are given by nanolab engineer to get the access of the instrument. Hitachi High-Tech SU9000 S(T)EM (NTNU Nano Lab). S(T)EM is used to perform on the sample to study the shapes and sizes that are less than 20nm because it is quite difficult to see the size on SEM Apreo. There are some parameters that we should consider while doing S(T)EM like acceleration voltage, magnification, and the detectors. The recommended parameters by the nano lab engineer are acceleration voltage 30 kV and acquiring bright field (BF) S(T)EM image with magnification of 50kX,100kX,150kX, and 200kX.

4.5.1 Working Principle of STEM

The working principle of STEM is that it uses a set of condenser lenses and an objective lens to accelerate electrons from a source that are focused at a specific place on the specimen. The objective angle limits the greatest angle of light in the input probe, and a collection of scan coils scans the material. The output of 27 detectors is used to create an image. Multiple detectors can be utilized to scan from various viewpoints. The transmitted beam is intercepted by a BF detector, while the transmitted beam is ringed by an annular dark field detector to gather dispersed electrons. STEM is depicted in the figure below.

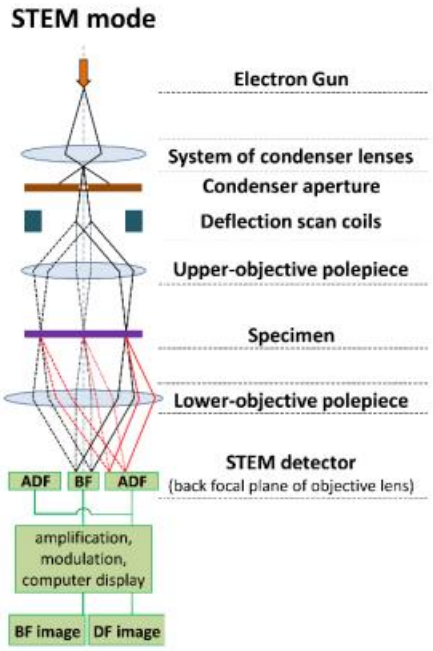

Figure 18 Working principle of S(T)EM

4.6 AFM Dimension Icon

For the surface morphology of hydrogel membranes, we used AFM dimension icon. Because this Scanning Probe Microscope performs all major SPM imaging techniques including PeakForce Tapping, ScanAsyst, TappingMode (air), Contact Mode, Lateral Force Microscopy, PhaseImaging, Lift Mode, Force Spectroscopy, Force Volume, Surface Potential, Torsional Resonance Mode, Piezoresponse Microscopy, Force Spectroscopy and MIRO without additional hardware. This AFM dimension icon perform imaging techniques on the sample that are placed inside the chamber and the range of imaging is up to 210mmin diameter / 15 mm thick

Figure 19 Dimension Icon Scanning Probe Microscope

4.6.1 Working Principle of AFM Dimension Icon

Before doing any experiment, we need to check the logbook to see the status of probe. If the probe is working properly, open the NanoScope programme and select your experiment category, such as which mode you want to use (we usually use ScanAsyst). After that, we must choose whether you are using ScanAsyst in air or ScanAsyst in fluid, and then load the experiment. After loading the experiment, after that click on align window to align the laser tip by zooming out or in when you see the laser spot on the optical field. You can also use the knobs to handle this. After that, we must find the focus by using focus up or focus down to focus on cantilever then the sum signal appears on the screen it should not be greater than 0.1 and voltage is around 4 KV. After that return from the alignment section and focus on the sample by using SPM head to make sure there is enough space between your sample and stage. After that rotate the sample where the laser light falls on your sample this is done by using the trackball after setting the laser light on the center of sample turn on the vacuum. Then check your initial parameter like Z range, scan rate, scan size and ScanAsyst auto control. After initial scan you can engage the experiment. After few minutes you can get 2 cannels height sensor and peak force error. Here you can capture images after that you can withdraw your experiment. You can also do offline image analysis by using nanoscope analysis software. Or there is another software Gwyddion

4.7 XRD

X-ray diffraction (Divici) was recorded to investigate the crystalline nature of AgNPs and fabricated bilayer hydrogels. Opening voltage of X-ray source was operated at 40Kv and 40 mA current, while scan speed and step size were 0.5s and 0.04s respectively with CuKα radiation having wavelength λ=1.5406 Å. In 1912, Max von Laue found that the crystalline substances act as three-dimensional diffraction grills for X-ray wavelengths corresponding to spacings in the plane. To analyze the atomic spacing and crystal structure, XRD is commonly employed. The main objectives of XRD are to identify the crystallinity of the material, differentiate between crystalline and amorphous forms, and calculate the percent crystallinity of the specimen

The following equation was used to calculate the average crystallite size.

$\tau=0.9\ \lambda/\beta\cos\theta$

where

τ denotes average crystallite size,

λ showing wavelength of X-rays,

β is the full width at half maximum,

θ is the Braggs angle

4.7.1 Working Principle of XRD

XRD analysis is based on the constructive interference of monochromatic X-rays with crystalline specimens. The X-rays produced by a cathode ray tube are filtered to produce monochromatic radiation. Collimation concentrates these rays, which are subsequently focused on the specimen. If the conditions are met, constructive interference occurs because of the interaction between these rays and the specimen. Bragg's Law is a relationship between the wavelength of electromagnetic radiation and the specimen's lattice spacing and diffraction angle. It is stated mathematically as[57, 58]

$$n\lambda = 2d \sin \theta$$

where,

n shows reflection, λ for wavelength, d for the spacing between crystal planes and θ is angle between normal to incident beam of lattice.

4.8 Fourier Transform Infrared Spectroscopy (FTIR)

FTIR analysis was done to specify the functional groups, and interfacial interactions through attenuated Total reflectance, FTIR (ATR-FTIR, BRUKER). The range for analysis was 4000-500 cm-1 with scanning frequency of 32 and resolution at 4 cm-1. The main objectives of FTIR is to recognize the organic, sometime inorganic and polymeric compounds, it also characterize unknown materials, it also help us to find the contamination in the material and in failure analysis it identify the oxidation, decomposition and uncured substance

4.8.1 Working Principle of FTIR

Molecules absorb light in the infrared range of the electromagnetic spectrum, where absorption is specific to the molecules' bonds. The frequencies are usually measured in the 4000-500 cm-1 range. The infrared area covers from 12800 to 10 cm-1 and is separated into three parts: near, mid, and far infrared. In near infrared region the frequency range is 12800-4000 (cm-1), mid infrared region the frequency range is 4000-200 (cm-1) and in far infrared region the frequency range is between 1000-50 (cm-1). The spectrum of infrared absorption is dependent on the vibrations of molecules. When a specimen is exposed to radiation, its molecules absorb specific wavelengths of radiation. The dipole mobility of specimen molecules is altered as a result. As a result, the energy level of the specimen molecule changes from ground to excited state. The frequency of absorption peak is determined by the energy gap. The dipole moments and energy level shifts influence the intensity change.

4.9 Thermogravimetric Analysis (TGA)

Thermal gravimetric analysis of hydrogel membranes, bilayer hydrogel membranes, and bilayer hydrogel membranes containing Nanoparticles of various sizes was performed at 20-650 C with a nitrogen gas flow rate of 40ml/min. The TGA's primary goals are to investigate the membrane's mass loss or weight loss in response to temperature changes. To test the thermal stability of the Bilayer hydrogel membranes, the entire reaction is carried out in a controlled environment.

TGA includes the following components: a balance, a furnace with programmable temperature control, and Netzsch TGA analysis software for analyzing the data. The analysis took 36 minutes at a temperature of 20-650 C, and the temperature of the furnace was calculated using a computer.

Figure 20 Netzsch TG209F1 TGA NTNU

4.9.1 Working principle of TGA

To start the TGA software first we need to open a new file in which we describe the material's identity and sample name, and then tare the crucible weight. After that, you must cut your sample and place it in the TGA, making sure that the weight of the sample is not less than 5mg, or you will not be able to get an accurate result. The next step is to program the temperature, such as the initial temperature, final temperature, and isothermal temperature. After that, you must choose the gas you will use (we will use N2 at a rate of 40ml/min), and then you must initiate the experiment. Analysis is performed by slowly increasing the temperature of the specimen in the furnace. The weight is measured by means of an analytical balance that is placed outside the furnace. The mass is observed as the loss of volatile matter occurs.

4.10 Moisture retention capability

To calculate the moister retention capability, the hydrogel membrane is cut into equal pieces and then weighed. After that the hydrogel membrane are put in an oven for 6h at 40C. the formula for MRC given below.[59]

Moisture retention capability (%) = [W_t/W_i] x 100

Where, W_i is the initial weight of the hydrogel before putting it in an oven and W_t is the weight of hydrogel after taken out from the oven.

4.11 Swelling test

In wound dressing application the ability of absorbing the water in the hydrogel is the important parameter. This exudes the absorbance form the wound and it is determined by swelling test. Swelling properties of the hydrogel were measured by initial and swollen weights of the hydrogels. For this test the hydrogels are immersed in the water for 48hr at room temperature. Then the swollen samples were taken out from the water and dried well and weighted. The sample was further dried in the vacuum oven at 60C and again reweighted.[60]

Swelling percent was determine by using the formula that is given below.

Degree of Swelling (%) = (W_d – W_s / $W_{d)}$ x 100

Where Wd is the weight of dry sample and Ws is the weight of Swollen sample of hydrogel.

4.12 Water Vapor Transmission Rate (WVTR)

WVTR was calculated according to the European pharmacopeia standards. The test was done in a round bottle with known diameter that was filled with 10 ml of MQ water, and the samples were fixed onto them. And the round bottle was covered with a Teflon tape to ensure the accuracy. After that the initial weight of the round bottle was recorded as W1. After that place the bottle in oven for 24 h at 40 ℃. After 24 h the bottle was taken out and the weight was recorded as W2. The WVTR was calculated by using the formula.[61] Where A is the permeation area of membranes.

$$\text{WVTR } (g/m^2.h) = \frac{(W_1 - W_2)}{A\ x\ t}$$

4.13 Antibacterial Activity Measurement

Disk diffusion method was used to measure the antibacterial activity measurement of the hydrogel's membranes. Bacterial strains of gram negative and gram positive was used for

this purpose of testing. The bacteria culture was prepared in a test tube by using the sonication bath at 37℃. The prepared bacterial was spread over the petri dish where the agar solution was already distributed. Furthermore, the sample was cut into 6mm round disk and positioned over the petri dish and we have to incubate that petri dish for 24 hr at 37℃. after 24 hr the inhabitation zone was formed around the disk that zone was measure by the vernier caliper. All the apparatus that was used in the measurement of antibacterial activity was autoclaved.

4.14 Cytotoxicity

The MTT assay is used to evaluate the metabolic activity and viability of cells. It is analyzed based on the ability of metabolically active/ live cells to convert water soluble MTT dye [3-(4,5-dimethylthiazol-2-yl)-2,5-diphenyltetrazolium bromide] into an insoluble formazan[62]. HEK-293 cells were used in order to evaluate cytotoxicity of (Hydrogel Membrane). These cells were obtained from ATCC (Manassas,VA). HEK-293 was cultured in its recommended medium DMEM supplemented with 10% fetal bovine serum (FBS) and 0.5% Penstrep (10,000 U/mL Penicillin, 10 µg /mL Streptomycin) to avoid bacterial contamination. Cells were incubated in standard conditions: 37 ℃, atmosphere of 95% air and 5% CO_2 and 100% humidity. Cells were used in experiment while they were in logarithmic phase of growth.

Different concentrations of membranes 100mg, 70mg, 30mg of samples were dissolved and incubated in PBS for 1 day, later the supernatant was collected and used for cytotoxicity analysis. Cells were seeded in a flat bottom 96 well microtiter plate for 24 hours. After 1 day they were exposed to prepared concentrations of sample for 24 hours (37 ℃ 5% CO_2, 100% humidity). All samples were tested in triplicates. Control cells did not receive any treatment. Following 24 hours incubation period media was aspirated and cells were incubated with 100 µl medium containing MTT dye in final concentration of 250 µg/ml of MTT. After adding MTT dye cells were incubated at 37 °C for 3 hours to let the formation of formazan-particles. Formazan particles were dissolved in DMSO (70µl) and then absorbance was measured at 580nm

Chapter 5

Result and Discussion

5.1 Design of Experiment Results

5.1.1 Model fitting of DOE when Silver Nitrate is Dropwise

To study the parameter that affects the size and morphology of NPs. The design of experiment was made using JMP software to investigate the influence of parameter like flowrate, PVP concentration, concentration of AgNO3 and reducing agent. After fitting the actual model to the whole design of experiment on JMP software, we found that reducing agent has most significant parameter due to which there is large deviation in the data set. To fit the multivariate linear model was adjudged using R^2 adjusted which was 0.86 in our case. For a good model it should be equal to or above 0.9. this show that model is statically significant enough to predict the influence of the parameter on deviation in datasets. the model is well-fit and has a P-Value of 0.0168. We can see that the change in the reducing agent has the most impact on the size and shape. After completing all 12 experiments, we notice how the size of the particles changes when the reducing agent is changed. When ascorbic acid is used as a reducing agent, we get sizes ranging from 1000 to 1800nm, when NaBH4 is used as reducing agent we get sizes in the range from 120nm to 190nm. And when Hydrazine is used, we get the sizes in the range from 125nm to 200nm.

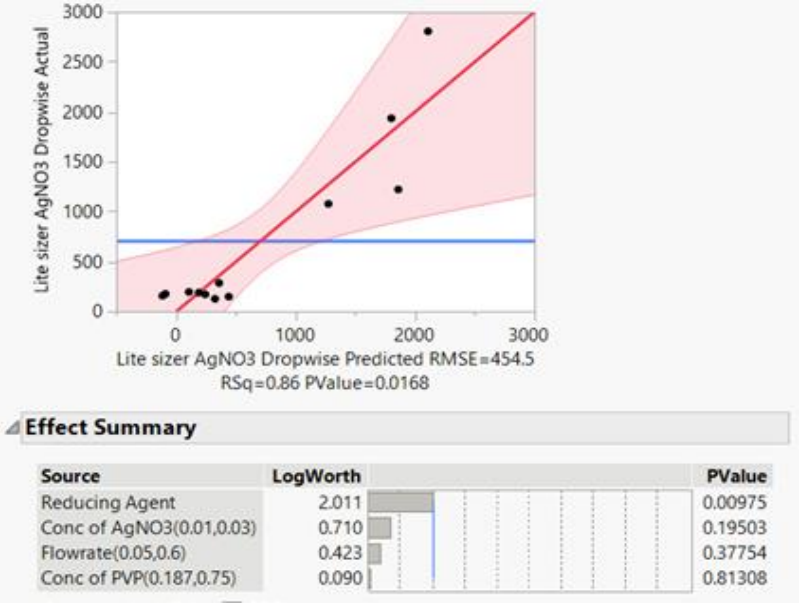

Figure 21 Model fitting of DOE experiments when AgNO3 is injected dropwise

5.1.2 Model fitting of DOE when Reducing Agent is Dropwise

To study the parameter that affects the size and morphology of NPs. The design of experiment was made using JMP software to investigate the influence of parameter like flowrate, PVP concentration, concentration of AgNO3 and reducing agent. After fitting the actual model to the whole design of experiment on JMP software, we found that reducing agent has most significant parameter due to which there is large deviation in the data set. To fit the multivariate linear model was adjudged using R^2 adjusted which was 0.89 in our case for a good model it should be equal to or above 0.9. this show that model is statically significant enough to predict the influence of the parameter on deviation in datasets. The model is well-fit and has a P-Value of 0.0081. We can see that the change in the reducing agent has the most impact on the size and shape. After completing all 12 experiments, we notice how the size of the particles changes when the reducing agent is changed. When ascorbic acid is used as a reducing agent, we get sizes ranging from 600 to 1800nm, when NaBH4 is used as reducing agent we get sizes in the range from 100nm to 150nm. And when Hydrazine is used, we get the sizes in the range from 100nm to 250nm.

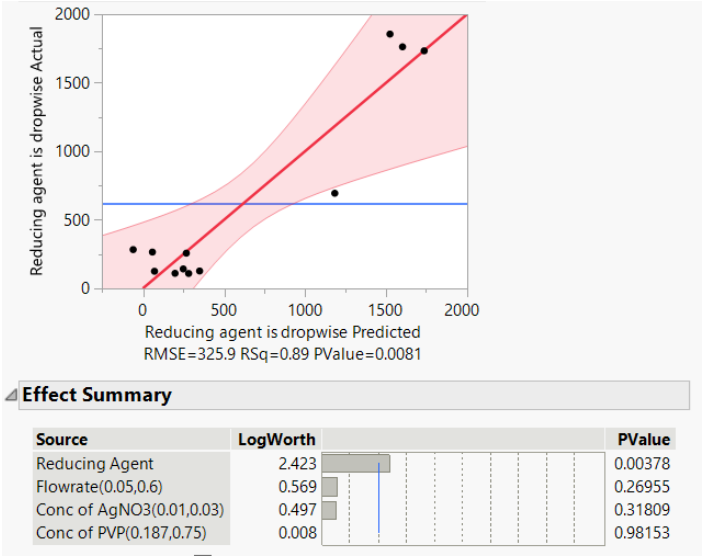

Figure 22 Model fitting of DOE experiments when reducing agent is injected dropwise

5.1.3 Conclusion of both Model

We concluded that the best model fitting was obtained when the reducing agent was dropwise based on reducing agent value and PValue and R^2 value after examining both models in JMP software. When the reducing agent is dropwise its PValue is 0.0081 and R^2 value is 0.89. When silver nitrate was dropwise, the reducing agent had the strongest influence and its PValue is 0.0168 and R^2 value is 0.86. According to PValue and R^2 value we found the that more accurate shape and size is found when the reducing agent is injected dropwise.

5.2 Nanoparticles Result When NaBH4 is Used as Reducing agent

5.2.1 UV Analysis

UV-Vis spectroscopy was used to investigate the formation of AgNPs. Many research papers propose that the dipole component of surface plasmonic resonance of silver nanoparticles is represented by the peak position of the absorption band between 380 and 500 nm in some publications. The LSPR peak was in the region of 380-410 nm after performing the DOE experiment with sodium borohydride, confirming the presence of AgNPs. The LSPR peak moves to a longer wavelength and broadens as the particle diameter increases. All the graphs are normalized but the parameters are change like flowrate, PVP concentration, concentration of AgNO3 and reducing agent. We have

changed these parameters to see that if we change these parameters, we are getting different shapes and sizes. After performing UV on both the scenario we observe that the LSPR peak are in the same ranges between 380-410nm.

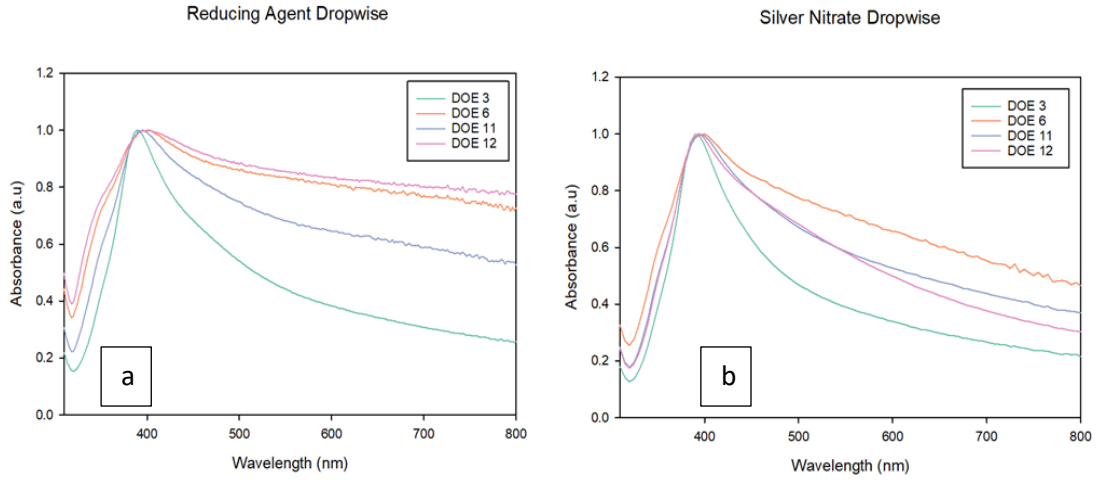

Figure 23 Schematic illustration of UV Vis graph when sodium borohydride is used a) Show four experiment of DOE 3,6,11,12 in which reducing agent is injected dropwise for preparation of AgNPs. b) show four experiment of DOE 3,6,11,12 in which silver nitrate is injected dropwise for preparation of AgNPs.

5.2.2 Lite Sizer

Because NaBH4 is a powerful reducing agent, we prepared it fresh to avoid degradation. First, PVP and AgNO3 are mixed, then NaBH4 is employed as a reducing agent. Because NaBH4 is a strong reducing agent, we can expect a high degree of supersaturation in a short period of time. Silver nuclei grow rapidly because of this high nucleation rate, and many silver NPs form spherical shapes. However, if the parameter is changed, we get varied sizes of DLS that are hydrodynamic sizes.[63, 64]

After analyzing the hydrodynamic size obtained by litesizer, we observed that when the reducing agent is injected dropwise, we obtain sizes in the range of 100nm to 285nm, with a zeta potential of – 31mV to –33mV. When silver nitrate is dropped dropwise, the size is in the range of 145nm to 285nm, and the zeta potential is in the range of -21mV to -32mV.

From both data, we can see that when the reducing agent is injected dropwise, we are getting better size and zeta potential.

Table 3. Comparison of sizes when NaBH4 is used for preparation of AgNPs

Sodium borohydride	**When reducing agent dropwise**	**Mean Zeta potential**	**When Silver Nitrate dropwise**	**Mean Zeta potential**
Experiment 3	109nm	-33.3 mV	147nm	-22.5 mV
Experiment 6	127nm	-31.9 mV	284nm	-32.9 mV
Experiment 11	125nm	-32.9 mV	194nm	-21.5 mV
Experiment 12	283nm	-33.2 mV	156nm	-23.0 mV

5.2.3 STEM Analysis of Nanoparticles

The morphology of AgNPs was characterized by S(T)EM. of Fig 24 (a, b, c, and d) show the images of DOE experiments in which reducing agent sodium borohydride is injected dropwise. These images show that the morphology of the particles is spherical, and the size of these particles are in the range of 10±5 nm we have use the image J software to analyze the size of the AgNPs in which sodium borohydride is used. We have change certain parameter in the DOE experiment in which sodium borohydride is used to see the change in morphology and size. Parameter that we change are flowrate, concentration of PVP, concentration of AgNO3 and the reducing agent but after analyzing the result we observe that majority of the shapes are spherical. The fig 24 (a, b, c, and d) was taken at 500nm.

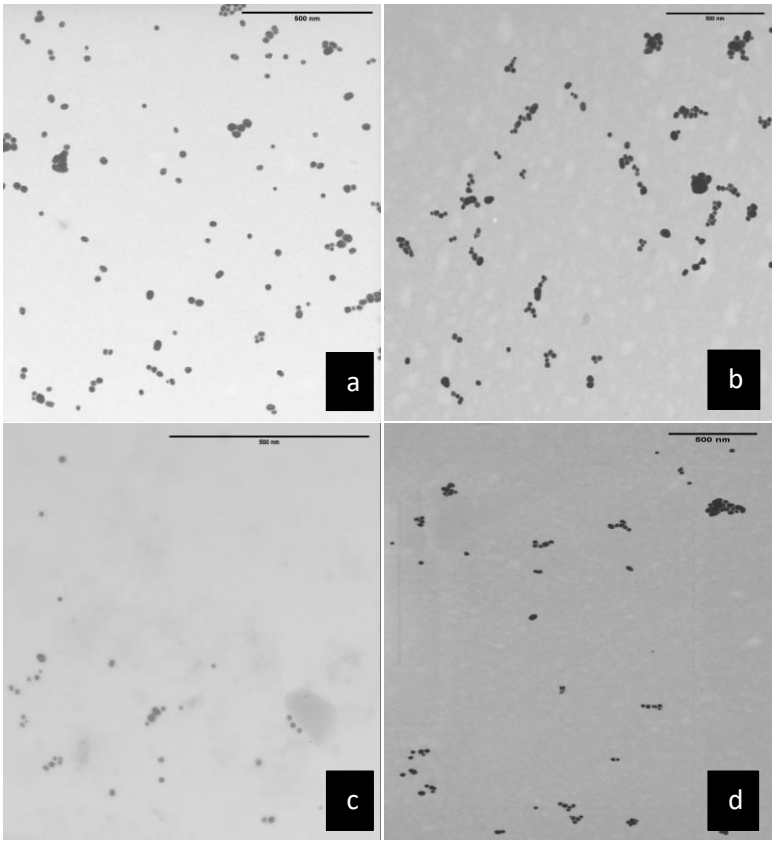

Figure 24 STEM image of silver nanoparticles in which NaBH4 is injected dropwise in the solution of AgNPs a) show the particle of AgNPs obtained by doing the experiment 3 of DOE, b) show the particle of AgNPs obtained by doing the experiment 6 of DOE, c) show the particle of AgNPs obtained by doing the experiment 11 of DOE, d) show the particle of AgNPs obtained by doing the experiment 3 of DOE

The AgNPs was characterized by S(T)EM. of Fig 25 (a, b, c, and d) show the images of DOE experiments in which silver nitrate was injected dropwise. These images show that the morphology of the particles is spherical, but the shape was not controlled, and the size of these particles are in the range of 10±5 nm we have use the image J software to analyze the size of the AgNPs in which silver nitrate is used dropwise. We have change certain parameter in the DOE experiment in which sodium borohydride is used to see the change in morphology and size. Parameter that we change are flowrate, concentration of PVP, concentration of AgNO3 and the reducing agent but after analyzing the result we observe that shapes are spherical but not controlled the fig 25 (a, b, c, and d) was taken at 500nm.

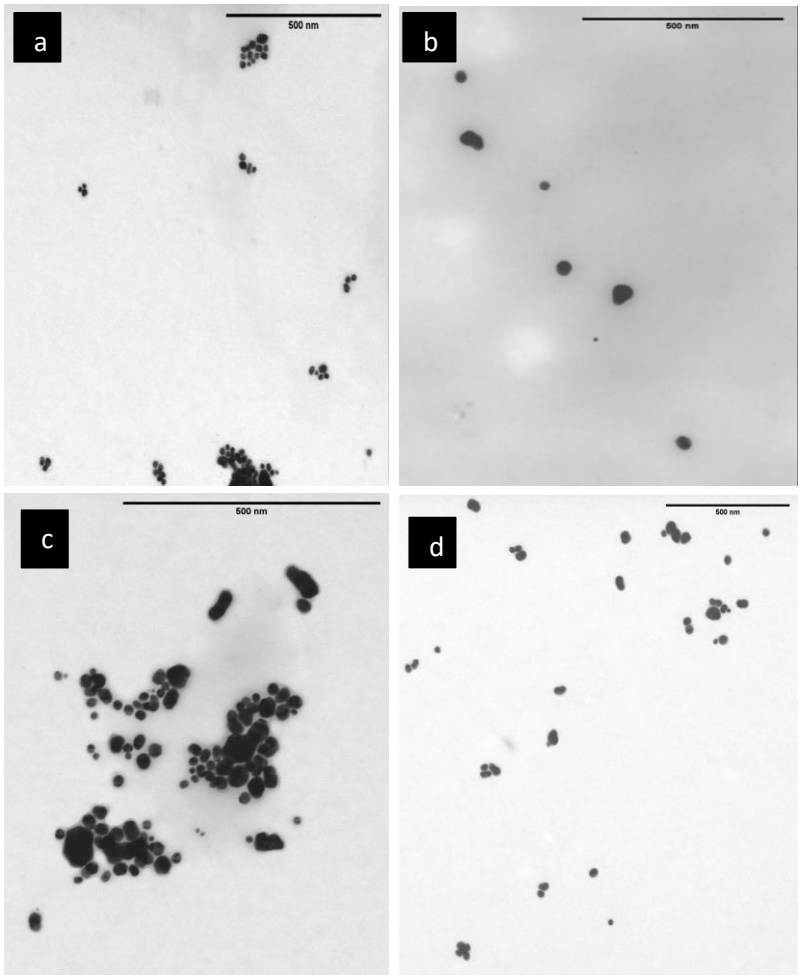

Figure 25 STEM image of silver nanoparticles in which silver nitrate is injected dropwise in the solution of AgNPs a) show the particle of AgNPs obtained by doing the experiment 3 of DOE, b) show the particle of AgNPs obtained by doing the experiment 6 of DOE, c) show the particle of AgNPs obtained by doing the experiment 11 of DOE, d) show the particle of AgNPs obtained by doing the experiment 3 of DOE

5.2.4 FTIR of Nanoparticles

Figure 26 show the infrared spectrum of silver nanoparticles (AgNPs) in which sodium borohydride is used as reducing agent, PVP as capping agent and AgNO3 as a salt precursor. The two-absorption band appear at 2956 and 2925 cm^{-1} these bands are due to symmetric and asymmetric vibration that is cause by **C – H** bond and there is strong bell shape absorption band at 1663cm^{-1} these band are form due to carbonyl group due to stretching vibration of **C = O** this caused by the presence of PVP. The other band at 1291, 1319,1374,1425,1440,1463, and 1495cm^{-1} are cause due to heterocyclic vibration in the PVP. While the other small band at 1019,845,736, and 649 1663cm^{-1} are due to **C – N** stretches**.** [65]

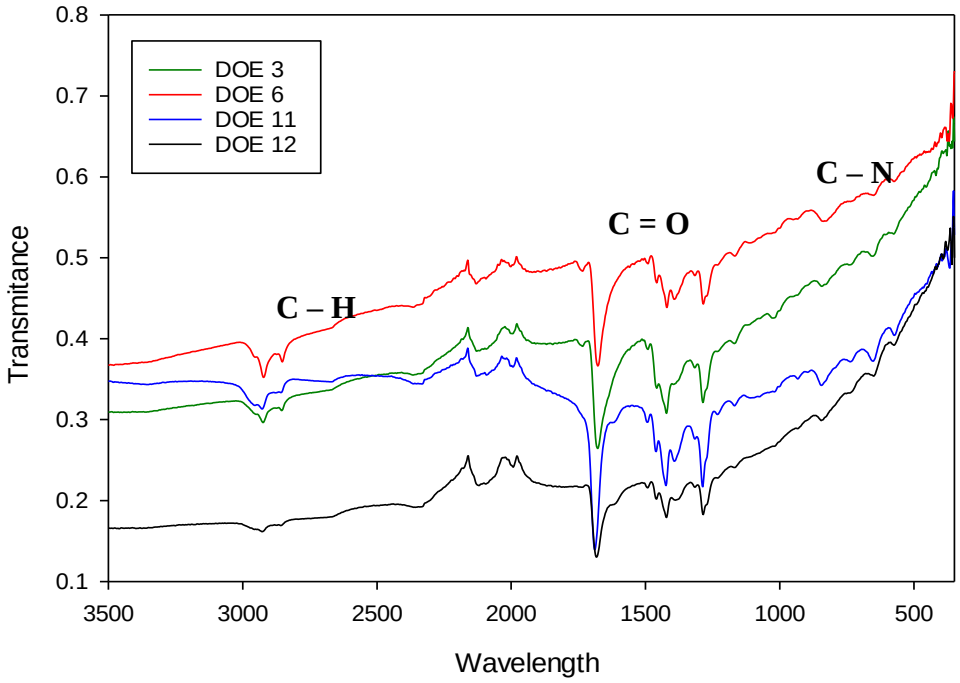

Figure 26 FTIR spectrum of Silver Nanoparticles when sodium borohydride is used a) green spectrum show the particle of AgNPs obtained by doing the experiment 3 of DOE, b) red spectrum show the particle of AgNPs obtained by doing the experiment 6 of DOE, c) blue spectrum show the particle of AgNPs obtained by doing the experiment 11 of DOE, d) black spectrum show the particle of AgNPs obtained by doing the experiment 3 of DOE

5.2.5 XRD Analysis

Phase analysis and crystal structure of prepared silver nanoparticles was characterized by XRD in figure 27. It features 4 peaks, but the strong peak was observed at 38 °, 43.5° ,

64.2°, 78.1° was relate to structure of silver. These peaks correspond to a crystal plane are (111), (200), (220), and (311) respectively. The average crystalline size was calculated by using the debye-sherrers.

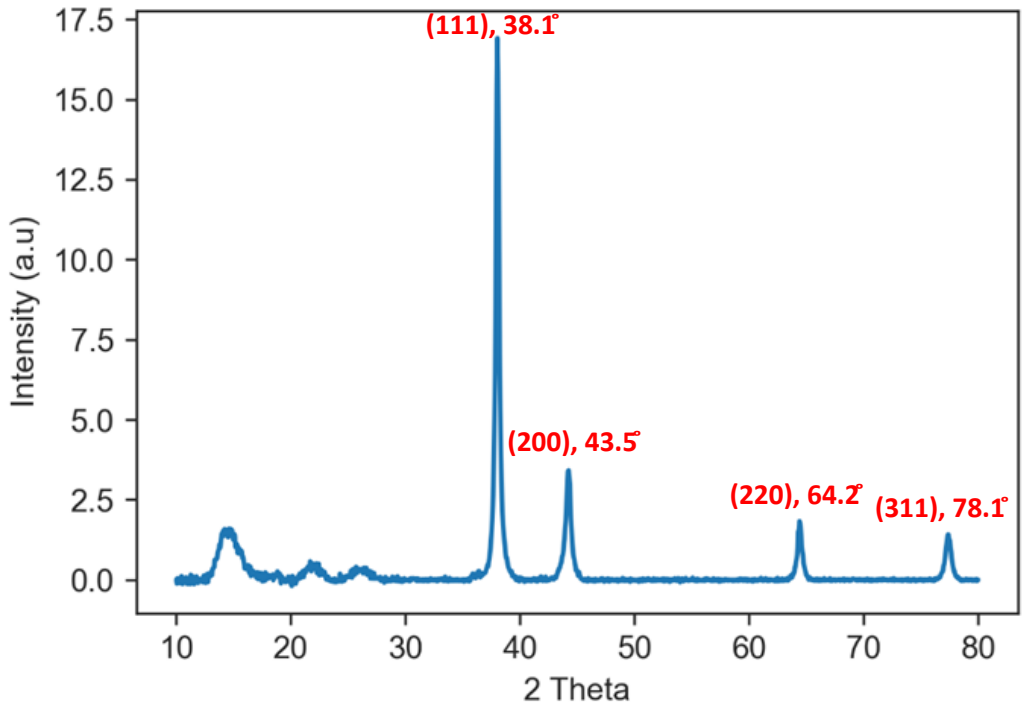

Figure 27 XRD analysis of silver nanoparticles in which NaBH4 is used as reducing agent

5.3 Nanoparticles Result when Hydrazine is used as reducing agent

5.3.1 UV Analysis

UV-Vis spectroscopy was used to investigate the formation of AgNPs. Many research papers propose that the dipole component of surface plasmonic resonance of silver nanoparticles are represented by the peak position of the absorption band between 380 and 500 nm in some publications. The LSPR peak was in the region of 380-410 nm after performing the DOE experiment with hydrazine confirm the presence of AgNPs. The LSPR peak moves to a longer wavelength and broadens as the particle diameter increases. All the graphs are normalized but the parameters are change like flowrate, PVP concentration, concentration of AgNO3 and reducing agent. We have changed these parameters to see that if we change these parameters, we are getting different shapes and sizes. After performing UV on the scenario, we observe that the LSPR peak are in the

same ranges between 390-420nm. It is confirmed that when we inject reducing agent dropwise, we are getting sharp LSPR peak as compared to other when silver nitrate is injected dropwise.

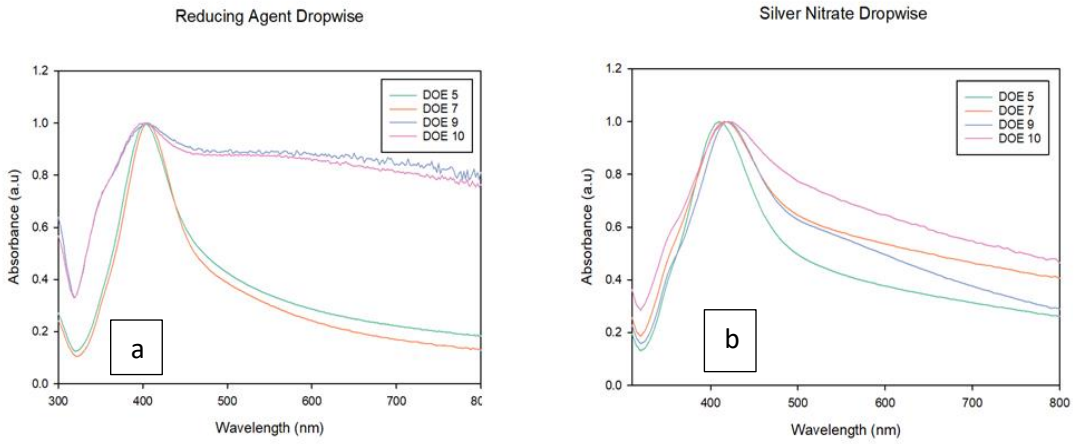

Figure 28 Schematic illustration of UV Vis graph when Hydrazine is used a) Show four experiment of DOE 3,6,11,12 in which reducing agent is injected dropwise for preparation of AgNPs. b) show four experiment of DOE 3,6,11,12 in which silver nitrate is injected dropwise for preparation of AgNPs.

5.3.2 Lite Sizer Analysis

After analyzing the hydrodynamic size obtained by litesizer, we observed that when the reducing agent is injected dropwise, we obtain sizes in the range of 110nm to 265nm, with a zeta potential of – 24mV to –32mV. When silver nitrate is dropped dropwise, the size is in the range of 126nm to 190nm, and the zeta potential is in the range of -22mV to -26mV. From both data, we can see that when the reducing agent is injected dropwise, we are getting better size and zeta potential.

Table 4. Comparison of sizes when hydrazine is used for preparation of AgNPs

Hydrazine	**When reducing agent dropwise**	**Mean Zeta potential**	**When Silver Nitrate dropwise**	**Mean Zeta potential**
Experiment 5	142 nm	-24.4 mV	126 nm	-22.6 mV
Experiment 7	110 nm	-27.5 mV	170 nm	-25.4 mV
Experiment 9	265 nm	-32.8 mV	176 nm	-24.1 mV
Experiment 10	256 nm	-32.1 mV	187 nm	-26.6 mV

5.3.3 SEM Apreo Analysis of Nanoparticles

The morphology of AgNPs was characterized by SEM Apreo. SEM analysis of Fig 29 (a, b, c, and d) show the images of DOE experiments in reducing agent hydrazine is injected dropwise. These images show the spherical structure of silver nanoparticles. These images show that the morphology of the particles is spherical, and the size of these particles are in the range of 45±5 nm we have use the image J software to analyze the size of the AgNPs in which hydrazine is used. We have change certain parameter in the DOE experiment in which hydrazine is used to see the change in morphology and size. Parameter that we change are flowrate, concentration of PVP, concentration of AgNO3 and the reducing agent but after analyzing the result we observe that majority of the shapes are spherical, and some aggregates are also observe but we can remove the aggregates by sonication. The fig 29-a was taken at low current of 25pA, and the voltage was 3.00 kV, A+B detectors are used with magnification 120000 and Z height was 3.1mm and the images were taken at 500nm. fig 29-b were taken at low current of 25pA, and the voltage was 5.00 kV, A+B detectors are used with magnification 167320 and Z height was 5.9mm and the images were taken at 500nm. fig 29-c were taken at low current of 25pA, and the voltage was 3.00 kV, A+B detectors are used with magnification 150000 and Z height was 3.1mm and the images were taken at 500nm. fig 29-d were taken at low current of 25pA, and the voltage was 5.00 kV, A+B detectors are used with magnification 65000 and Z height was 3.1mm and the images were taken at 1µm.

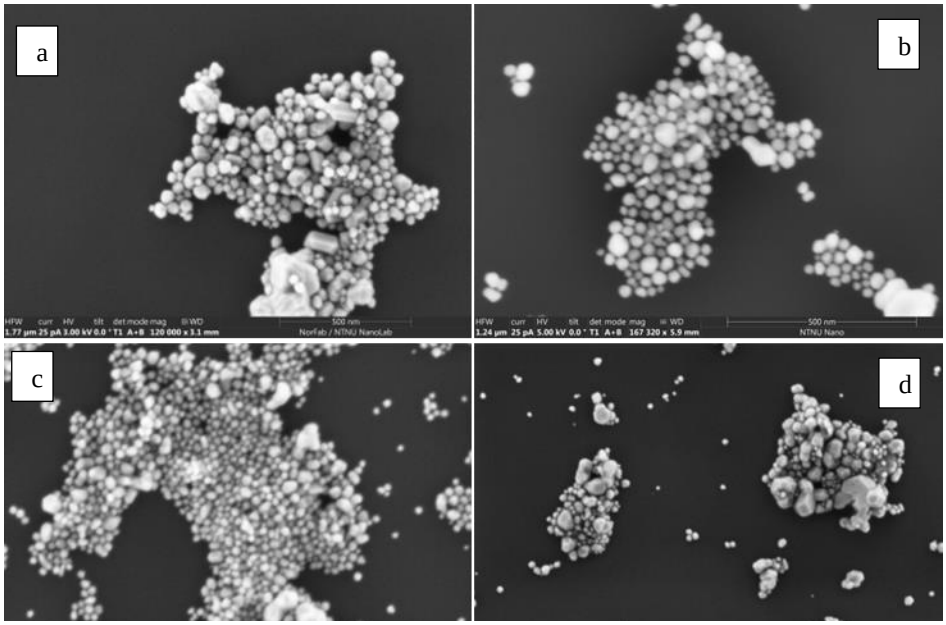

Figure 29 SEM image of silver nanoparticles in which hydrazine is injected dropwise in the solution of AgNPs a) show the particle of AgNPs obtained by doing the experiment 5 of DOE, b) show the particle of AgNPs obtained by doing the experiment 7 of DOE, c) show the particle of AgNPs obtained by doing the experiment 9 of DOE, d) show the particle of AgNPs obtained by doing the experiment 10 of DOE

Similarly, the SEM analysis of Fig 30 (a, b, c, and d) show the images of DOE experiment in which Silver Nitrate is injected dropwise. So that we can see which gives the best shape and size of AgNPs. Fig 30 (a, b, c, and d) shows the spherical structure of silver nanoparticles, but the shape was not controlled when the silver nitrate is injected dropwise more aggregates are formed. These images show that the morphology of the particles is spherical, and the size of these particles are in the range of 40±10 nm we have use the image J software to analyze the size of the AgNPs in which hydrazine is used. We have change certain parameter in the DOE experiment in which hydrazine is used to see the change in morphology and size. Parameter that we change are flowrate, concentration of PVP, concentration of AgNO3 and the reducing agent but after analyzing the result we observe that some spherical shapes of silver NPs was observed but aggregates are also there, and size was not controlled. The fig 30-a was taken at low current of 25pA, and the voltage was 3.00 kV, A+B detectors are used with magnification 100000 and Z height was 3.0mm and the images were taken at 1µm. fig 30-b were taken at low current of 25pA, and the voltage was 3.00 kV, A+B detectors are used with magnification 120000 and Z height was 3.0mm and the images were taken at 500nm. fig 30-c were taken at low current

of 25pA, and the voltage was 3.00 kV, A+B detectors are used with magnification 150000 and Z height was 3.1mm and the images were taken at 500nm. fig 30-d were taken at low current of 25pA, and the voltage was 3.00 kV, A+B detectors are used with magnification 100000 and Z height was 3.1mm and the images were taken at 1µm. only fig 30-c show the more spherical particles as compared to other three experiments of DOE.

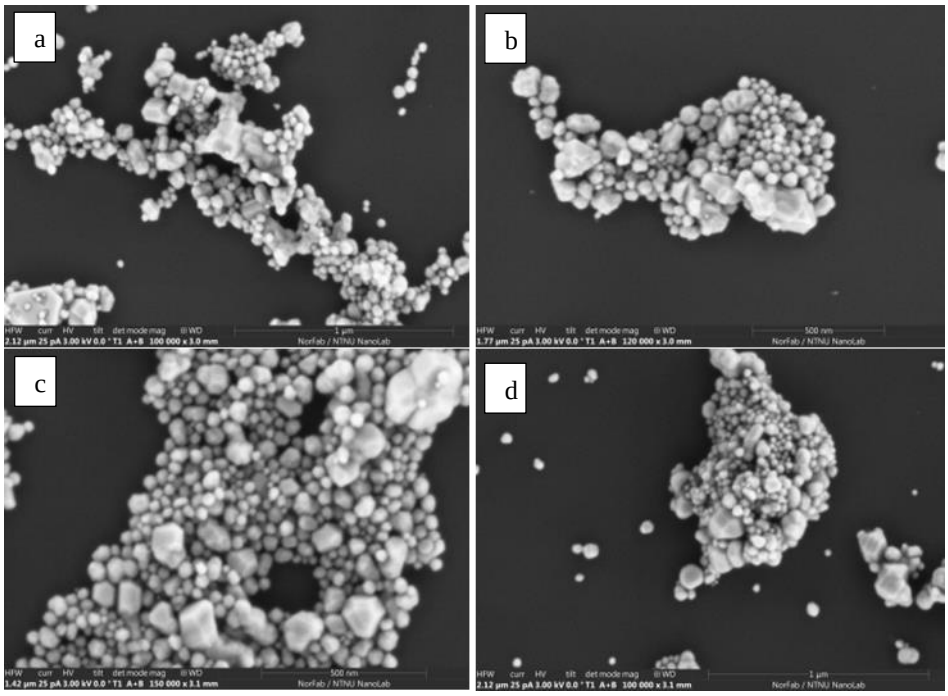

Figure 30 SEM image of silver nanoparticles in which Silver Nitrate is injected dropwise in the solution of AgNPs a) show the particle of AgNPs obtained by doing the experiment 5 of DOE, b) show the particle of AgNPs obtained by doing the experiment 7 of DOE, c) show the particle of AgNPs obtained by doing the experiment 9 of DOE, d) show the particle of AgNPs obtained by doing the experiment 10 of DOE

After analyzing both the experiment in which reducing agent is dropwise and in which silver nitrate is dropwise and we observe that best results are those in which reducing agent is dropwise they give the controlled size and shape.

5.3.4 FTIR of Nanoparticles

Figure 31 show the infrared spectrum of silver nanoparticles (AgNPs) in which hydrazine is used as reducing agent, PVP as capping agent and AgNO3 as a salt precursor. The two-absorption band appear at 2956 and 2925 cm^{-1} these bands are due to symmetric and

asymmetric vibration that is cause by **C – H** bond and there is strong bell shape absorption band at 1663cm^{-1} these band are form due to carbonyl group due to stretching vibration of **C = O** this caused by the presence of PVP. The other band at 1291, 1319,1374,1425,1440,1463, and 1495cm^{-1} are cause due to heterocyclic vibration in the PVP.

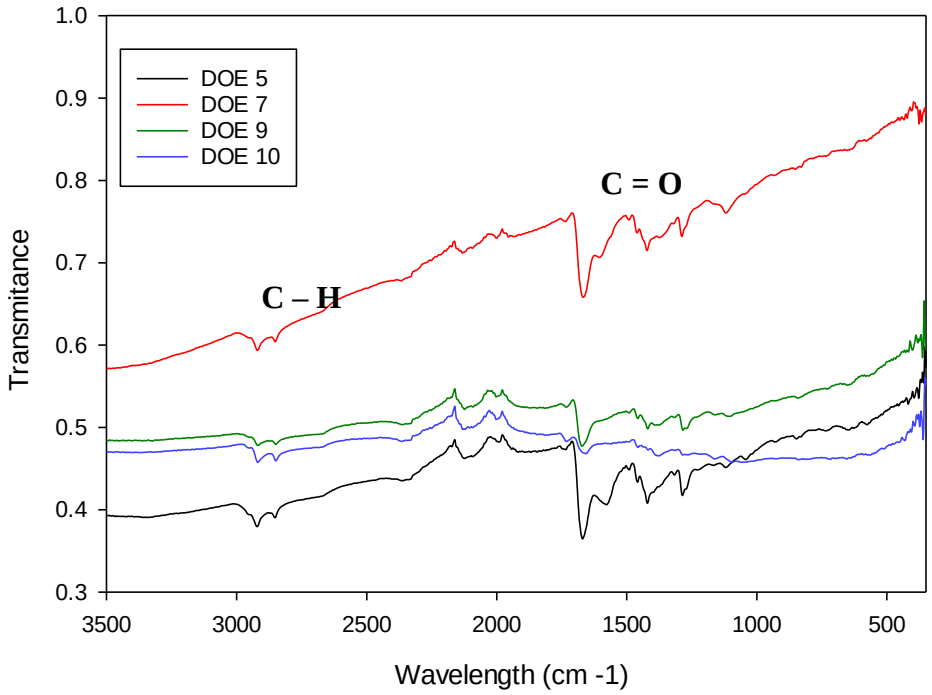

Figure 31 FTIR spectrum of Silver Nanoparticles when Hydrazine is used a) black spectrum show the particle of AgNPs obtained by doing the experiment 5 of DOE, b) red spectrum show the particle of AgNPs obtained by doing the experiment 7 of DOE, c) green spectrum show the particle of AgNPs obtained by doing the experiment 9 of DOE, d) blue spectrum show the particle of AgNPs obtained by doing the experiment 10 of DOE

5.3.5 XRD of Nanoparticles

Phase analysis and crystal structure of prepared silver nanoparticles was characterized by XRD in figure 27. It features 4 peaks, but the strong peak was observed at 38 °, 43.5°, 64.2°, 78.1° was relate to structure of silver. These peaks correspond to a crystal plane are (111), (200), (220), and (311) respectively.

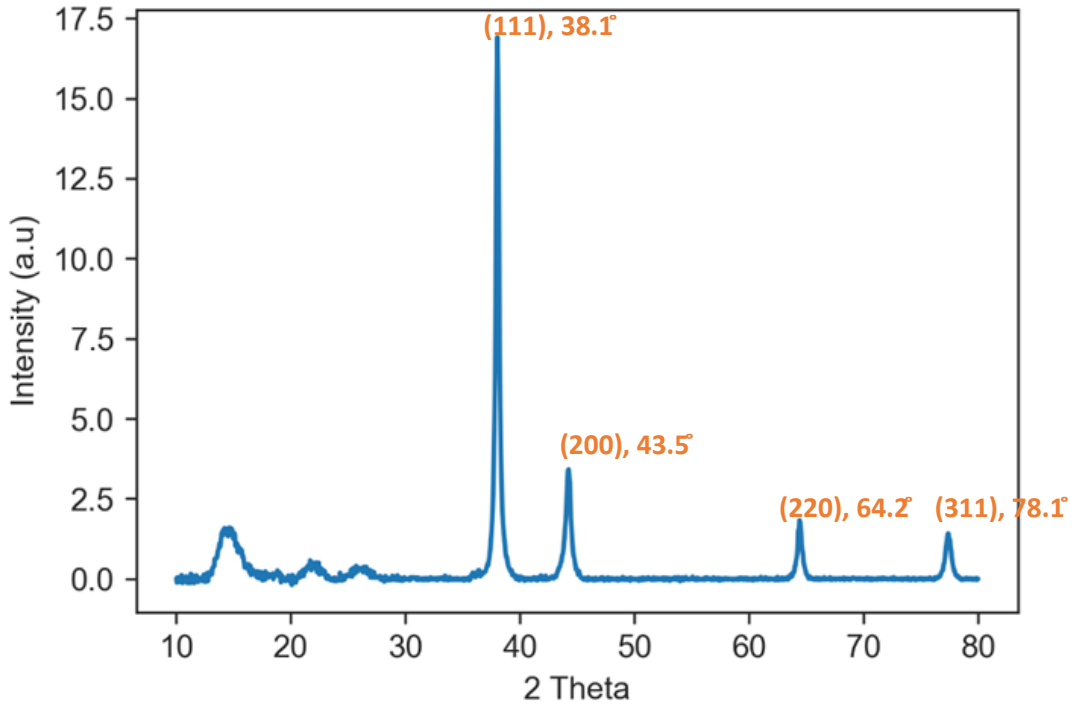

Figure 32 XRD analysis of silver nanoparticles in which hydrazine is used as reducing agent

5.4 Nanoparticles Results when Ascorbic acid is used as reducing agent

5.4.1 UV Analysis

Form the UV analysis we see that no of localized surface plasmonic resonance (LSPR) peak was observed because the size of the particle is too big and they are quickly settling down so when the UV light is passed through cuvette the particles was settled down so we cannot confirm that our particles are form or not so we cannot take that result in further studies because ascorbic acid is slow reducing agent and there is chances that it has not reduce the salt precursor and our particles was not formed.

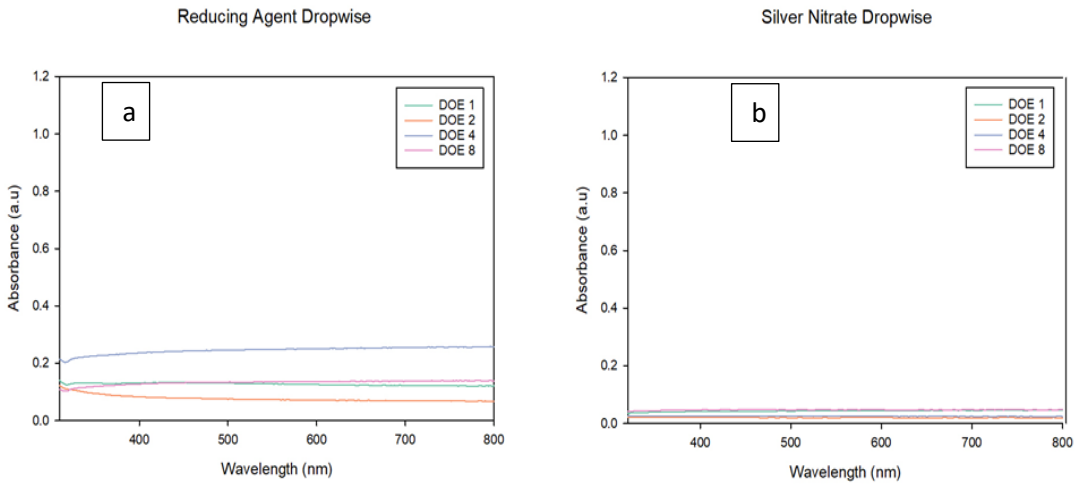

Figure 33 Schematic illustration of UV Vis graph when Ascorbic acid is used a) Show four experiment of DOE 1,2,4 and 8 in which reducing agent is injected dropwise for preparation of AgNPs. b) show four experiment of DOE 1,2,4 and 8 in which silver nitrate is injected dropwise for preparation of AgNPs

5.4.2 Lite Sizer Analysis

After analyzing the hydrodynamic size obtained by litesizer, we observed that when the reducing agent is injected dropwise, we obtain sizes in the range of 690nm to 1855nm, with a zeta potential of – 29mV to –33mV. When silver nitrate is dropped dropwise, the size is in the range of 1076nm to 2807nm, and the zeta potential is in the range of -33mV to -39mV. From both data, we can see that when the reducing agent is injected dropwise, we are getting better but when silver nitrate is dropwise, we are getting better zeta potential.

Table 5. Comparison of sizes when ascorbic acid is used for preparation of AgNPs

Ascorbic acid	**When reducing agent dropwise**	**Mean Zeta potential**	**When Silver Nitrate dropwise**	**Mean Zeta potential**
Experiment 1	694 nm	-29.9 mV	1076 nm	-33.6 mV
Experiment 2	1855 nm	-31.9 mV	1935 nm	-33.2 mV
Experiment 4	1762 nm	-33.1 mV	1221 nm	-39.9 mV
Experiment 8	1733 nm	-29.6 mV	2807 nm	-33.8 mV

5.4.3 SEM Apreo Analysis of Nanoparticles

We can see that the size was not controlled when we inject silver nitrate dropwise because some aggregated structure was observed, while when we inject reducing agent dropwise

we see a better image but the shape was still not controlled because the particles were quickly settling down and multiple shapes was observed we don't see any localized surface plasmonic resonance (LSPR) peak in UV that confirms that we have prepared the silver nanoparticles so we can't use them in our experiments.

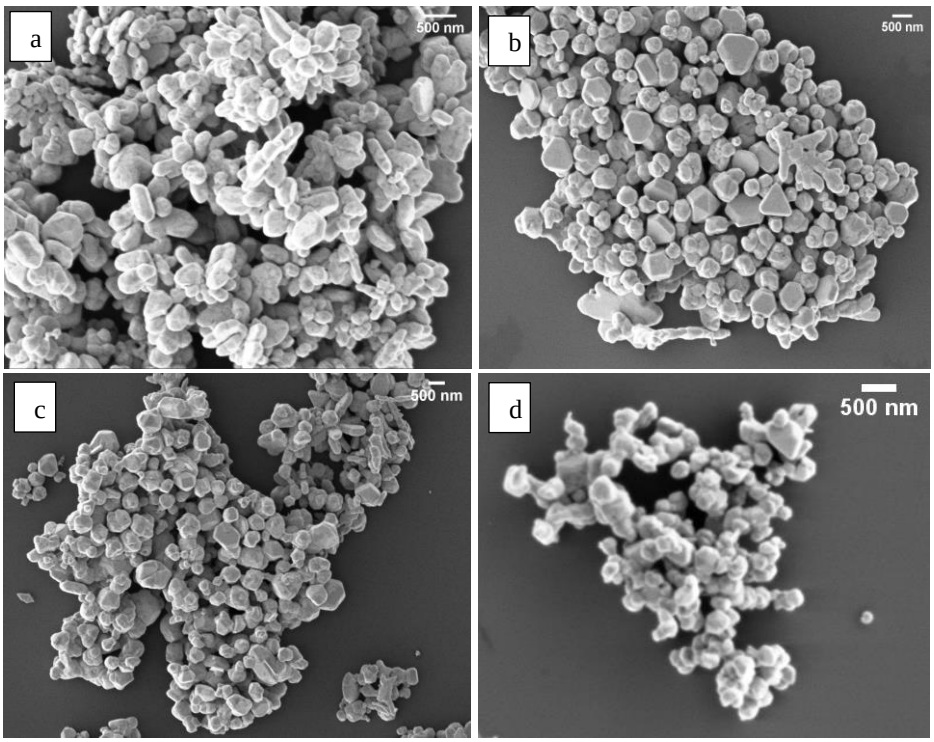

Figure 34 SEM image of silver nanoparticles in which ascorbic acid is injected dropwise in the solution of AgNPs a) show the particle of AgNPs obtained by doing the experiment 1 of DOE, b) show the particle of AgNPs obtained by doing the experiment 2 of DOE, c) show the particle of AgNPs obtained by doing the experiment 4 of DOE, d) show the particle of AgNPs obtained by doing the experiment 8 of DOE.

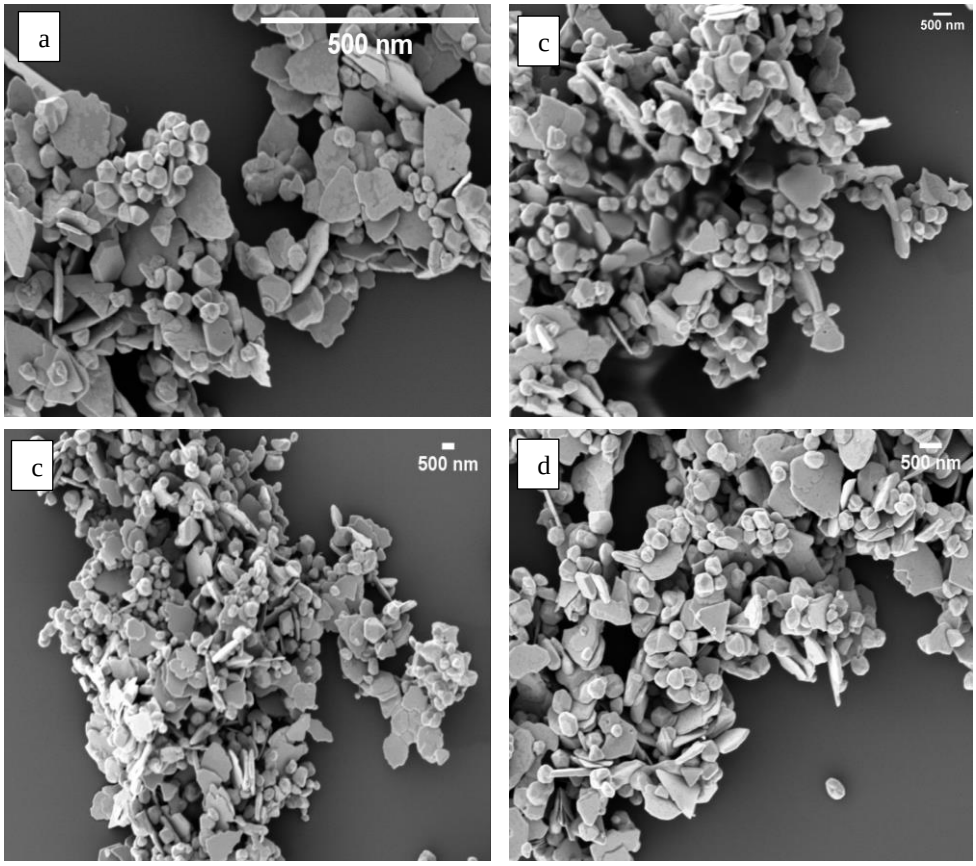

Figure 35 SEM image of silver nanoparticles in which silver nitrate is injected dropwise in the solution of AgNPs a) show the particle of AgNPs obtained by doing the experiment 1 of DOE, b) show the particle of AgNPs obtained by doing the experiment 2 of DOE, c) show the particle of AgNPs obtained by doing the experiment 4 of DOE, d) show the particle of AgNPs obtained by doing the experiment 8 of DOE

5.5 Seeded growth synthesis

We use seeded growth method to increase the size of silver nanoparticles to get different ranges of silver nanoparticles originally, we use the seed of experiment 3 in which sodium borohydride is used as reducing agent and the size of these particles was 10±5 nm S(T)EM size that was calculated by using image J software after counting 200 particles. After performing the seeded growth synthesis, we get the bigger size particles we use the seed in three different ratios like 100ul, 250ul and 500ul of the original seed and its hydrodynamic size was of seed is 109nm in fig 36-a. After adding 100ul seed size is 130nm in fig 36-b, after adding 250ul seed size is 140nm in fig 36-c, and after adding 500ul seed size is 163nm in fig 36-d this was analyzed by lite sizer.

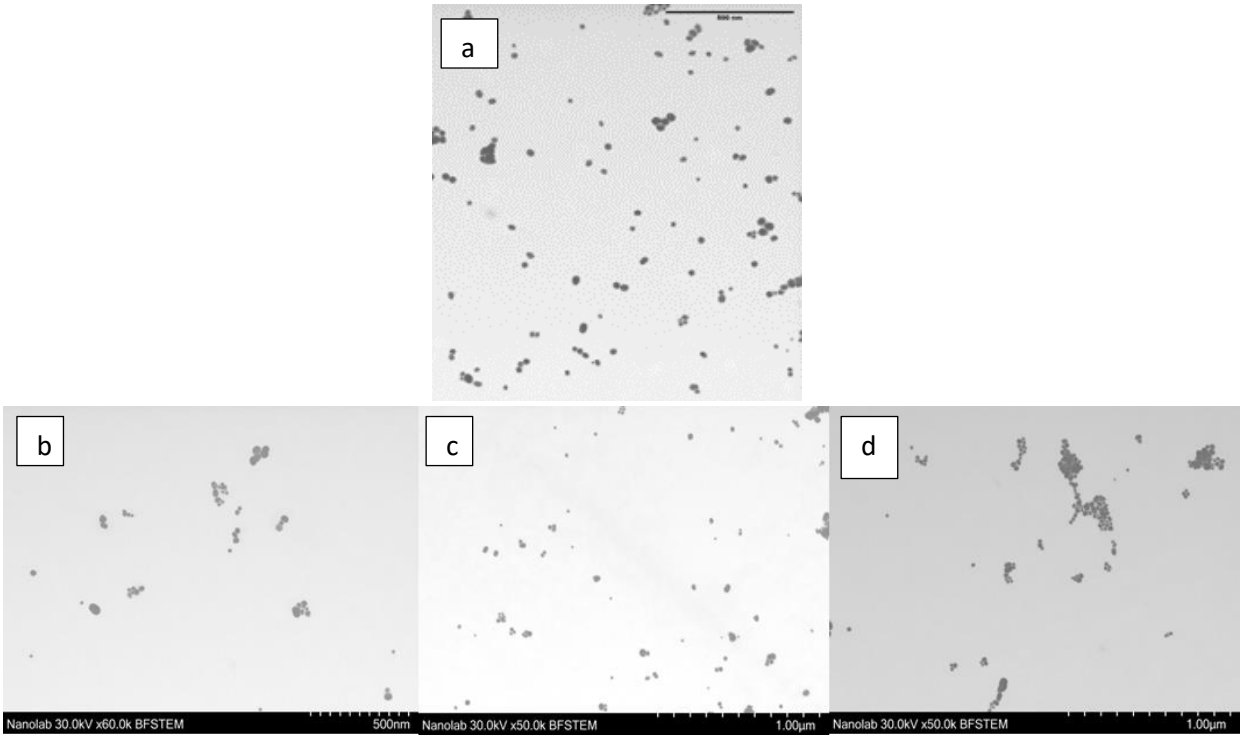

Figure 36 Seeded growth synthesis a) original seed of experiment 3 DOE in which NaBH4 is injected dropwise b) 100ul seed of experiment 3 of DOE in which NaBH4 is injected dropwise c) 250ul seed of experiment 3 DOE in which NaBH4 is injected dropwise and d) 500ul seed of experiment 3 of DOE in which NaBH4 is injected dropwise

After analyzing all the images from S(T)EM we found the best image was observe when the seed ratio is 250ul and the STEM size was increased from 10 ± 5nm to 25 ± 5 nm

5.6 Membranes Results

5.6.1 SEM Apreo Analysis

After the bilayer is prepared by solvent casting method, we must confirm that the bilayer is formed so that we can incorporate the silver nanoparticles in bilayer hydrogel membrane. For this we must cut our membrane with liquid nitrogen to analyze the morphology of bilayer by doing the cross section of membrane in SEM Apreo. All the characterization has been used in NTNU Nano lab for the analysis of bilayer hydrogel membrane we use ETD detectors in SEM mode and the current that was used is 0.40nA, HV voltage was 3.00KV, magnification is 574X, Z height was 3.4mm and that image was taken at 300µm. From the SEM image we clearly see that morphology of both layer is

different that confirm that bilayer is formed, and the thickness of bilayer is 190 ± 5µm and the thickness of each layer is 90 ± 5µm the top layer is chitosan, and the bottom layer is PVA.

5.6.1.1 SEM of Bilayer

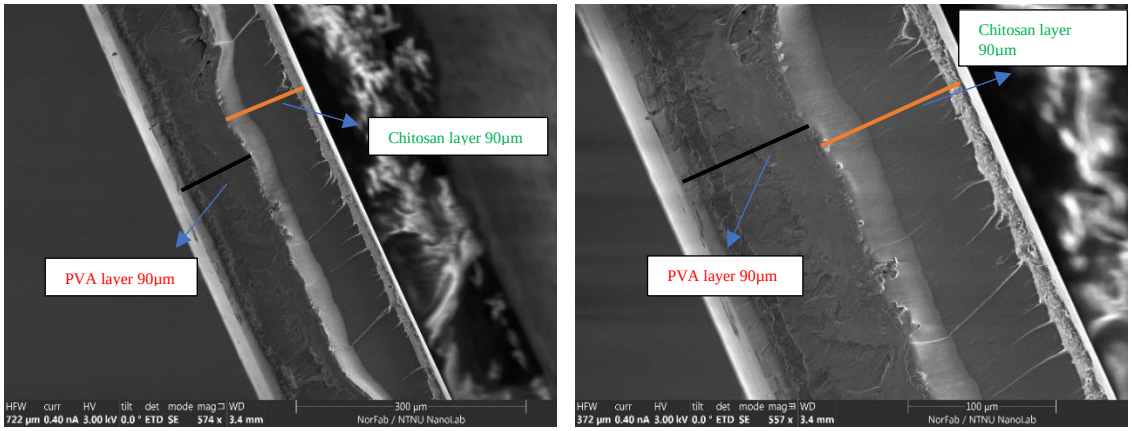

Figure 37 SEM of Bilayer hydrogel membrane of PVA/Chitosan

5.6.1.2 SEM of Bilayer Nanoparticles incorporated

After the confirmation of bilayer, we have to incorporate the silver nanoparticles of different sizes like 10 ±5nm, 25± 5nm and 50± 5nm in bilayer hydrogel membrane. After the incorporation of silver nanoparticles, we must analyze the hydrogel membrane for this we must cut our membrane with liquid nitrogen to analyze the morphology of bilayer in which nanoparticles are present by doing the cross section of membrane in SEM Apreo we see that morphology of both layer is different but there is slightly change in PVA and Chitosan structure due to incorporation of silver nanoparticles. Bilayer hydrogel membrane in which the nano particles are incorporated we use ETD detectors in SEM mode for cross section of the image and the current that was used is 0.40nA, HV voltage was 3.00KV, magnification is 187X, Z height was 5.2mm and that image was taken at 500µm and the thickness of bilayer is 190 ± 5µm and the thickness of each layer is 90 ± 5µm the top layer is chitosan, and the bottom layer is PVA. While observing the top surface of membrane we that that there are some rough structures that show in the fig 1b that confirm the presence of silver nanoparticles same ETD detector is used, current was 0.40nA, HV voltage 3.00KV, the stage was tilt at 13-degree, magnification was 3084X, Z height was 6.1mm and the image was taken at 30µm.

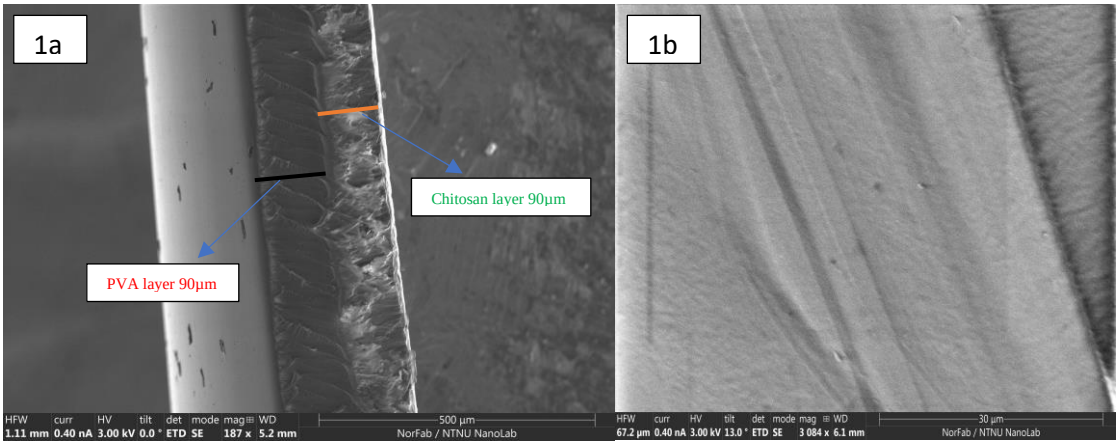

Figure 38 SEM of bilayer hydrogel membrane of PVA/Chitosan in which AgNPs are incorporated 1a) show the cross-section image of bilayer membrane,1b) show the top surface of bilayer hydrogel membrane

5.6.2 XRD Analysis

The XRD pattern of pure PVA powder and pure chitosan powder show various peak of its constitutes. Furthermore, they are compared with PVA membrane and bilayer hydrogel membrane. In fig 40 we see two peaks for pure PVA one is sharp peak at 19˚and second at 40˚. And in case of pure chitosan powder, we get the single peak at 20˚. After that we compare these peaks after preparing pure PVA membrane and bilayer membrane of PVA/chitosan and we are getting similar sharp peak at 19˚for PVA and sharp peak of chitosan at 20˚peak. The peak that is ~20˚shows the characteristic peak of chitosan. There is a single peak in bilayer membrane because the intermolecular interaction between both the polymers [66]

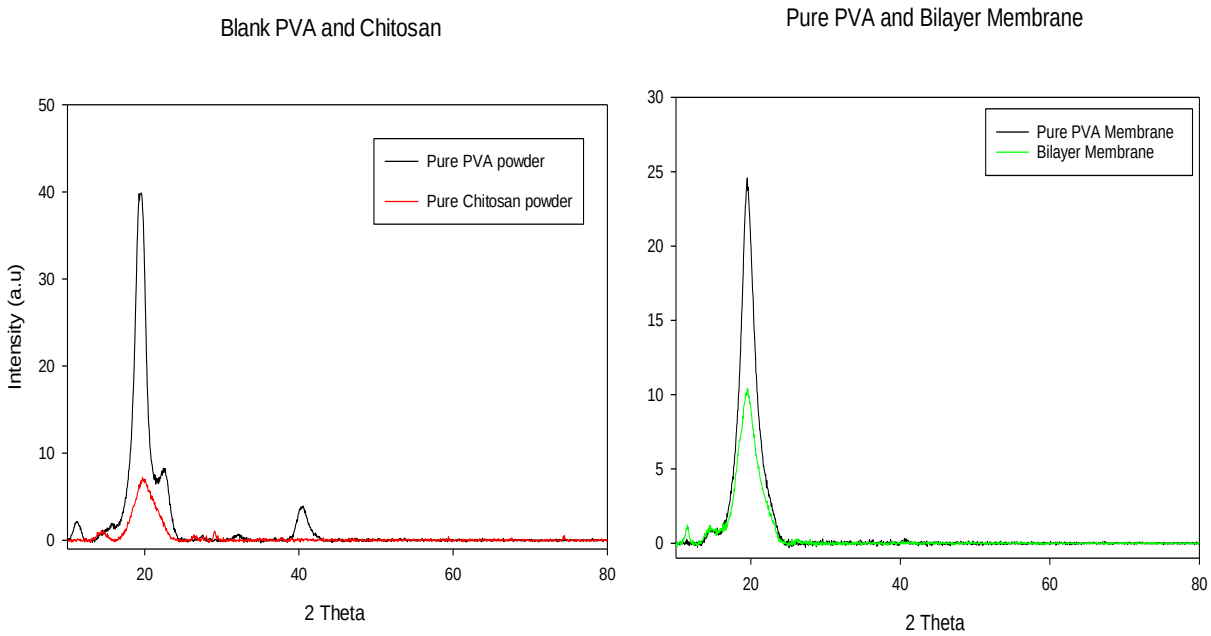

Figure 39 Comparison blank powder and hydrogel membrane

Figure 41 depicts the XRD pattern of bilayer hydrogel membrane in which 10±5nm AgNPs are incorporated the shape of these particles is spherical and the quantity of AgNPs is constant is every membrane. The silver nanoparticles show features 4 peaks, but the strong peak was observed at 38 °, 43.5°, 64.2°, 78.1° was relate to structure of silver. These peaks correspond to a crystal plane are (111), (200), (220), and (311) respectively. After incorporation we the broad peak of PVA and chitosan at 20° and some small peaks at 38°,43.5 °,64.2°,78.1° at is due to presence of silver nanoparticles in membrane the quantity of these AgNPs is less so we observe small peaks

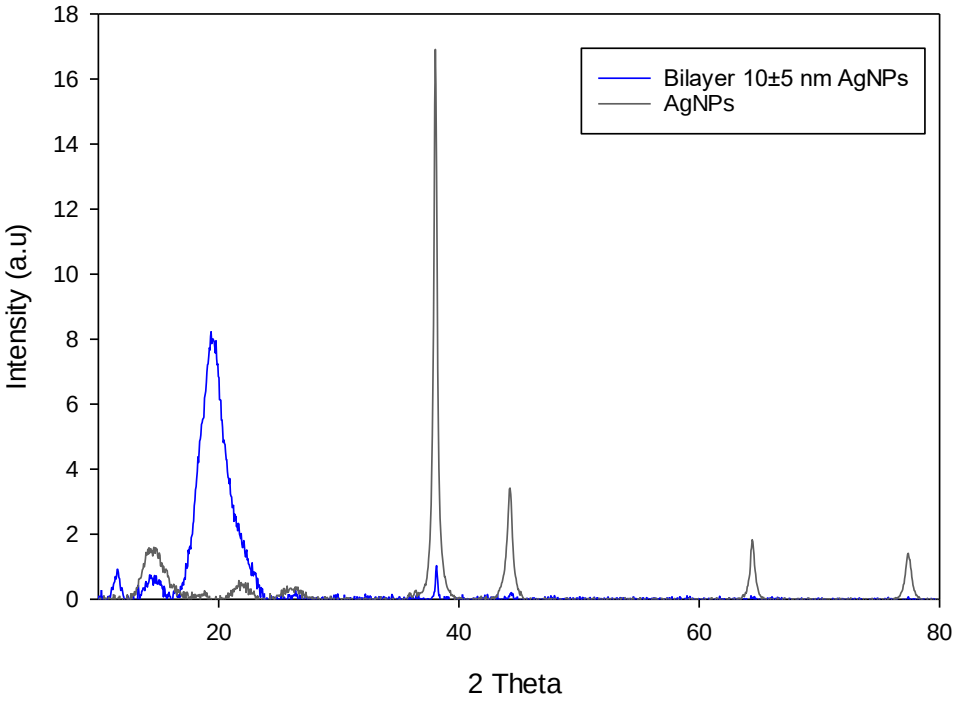

Figure 40 Bilayer 10±5 nm AgNPs

Figure 42 depicts the XRD pattern of bilayer hydrogel membrane in which 25±5nm AgNPs are incorporated the shape of these particles is spherical and the quantity of AgNPs is constant is every membrane. The silver nanoparticles show features 4 peaks, but the strong peak was observed at 38 °, 43.5°, 64.2°, 78.1° was relate to structure of silver. These peaks correspond to a crystal plane are (111), (200), (220), and (311) respectively. So, after incorporation we the broad peak of PVA and chitosan at 20° and some small peaks at 38°,43.5 °,64.2°,78.1° at is due to presence of silver nanoparticles in membrane the quantity of these AgNPs is less so we observe small peaks

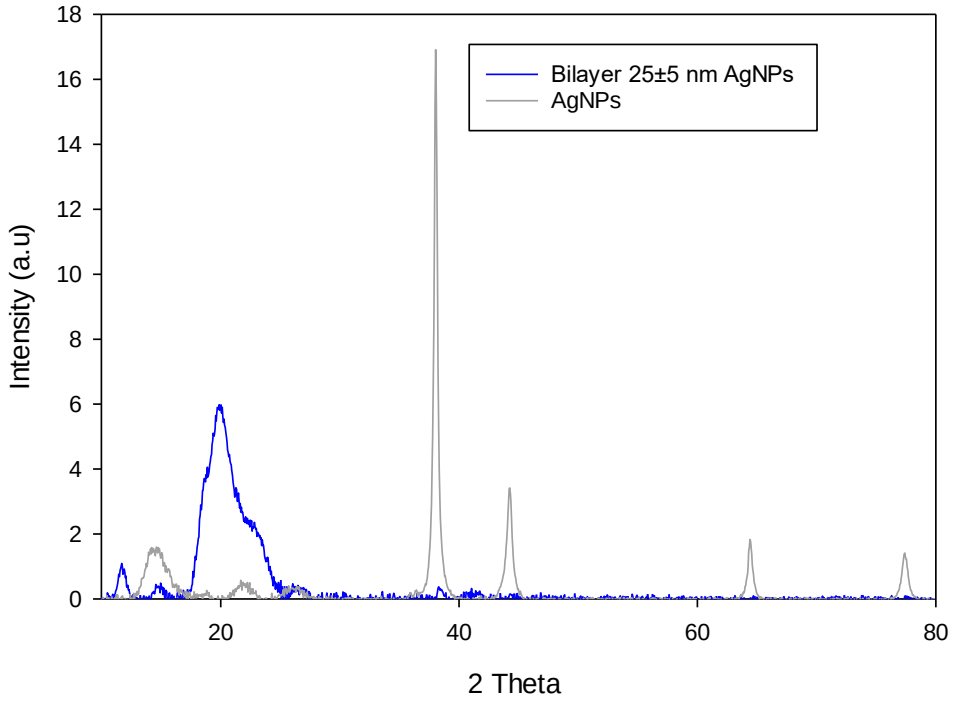

Figure 41 Bilayer 25±5 nm AgNPs

Figure 43 depicts the XRD pattern of bilayer hydrogel membrane in which 45±5nm AgNPs are incorporated the shape of these particles is spherical and the quantity of AgNPs is constant is every membrane. The silver nanoparticles show features 4 peaks, but the strong peak was observed at 38 °, 43.5°, 64.2°, 78.1° was relate to structure of silver. These peaks correspond to a crystal plane are (111), (200), (220), and (311) respectively. So, after incorporation we the broad peak of PVA and chitosan at 20° and some small peaks at 38°,43.5 °,64.2°,78.1° at is due to presence of silver nanoparticles in membrane the quantity of these AgNPs is less so we observe small peaks

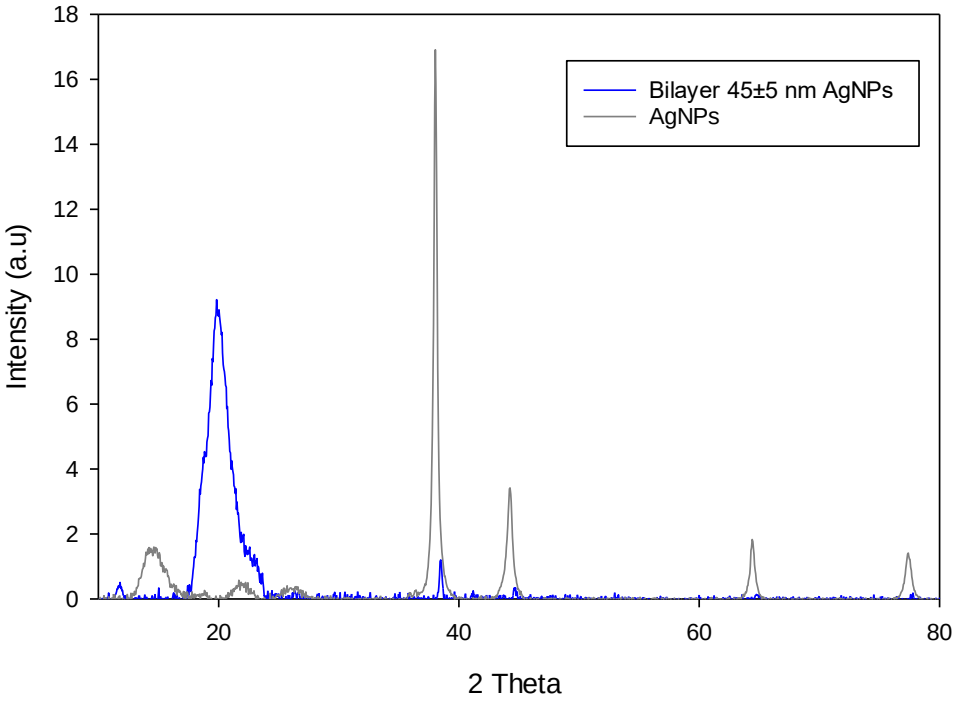

Figure 42 Bilayer 45±5 nm AgNPs

5.6.3 AFM Analysis

Figure 44 show the AFM dimension icon image of pure PVA membrane and bilayer hydrogel membrane fig 44-(1a and 1b) show the image of pure PVA membrane these pictures show the image scan from 241nm to 100nm in height sensor and 80.7pN to -81.1pN in peak force error and the image was taken at 40 nm. fig 44-(2a and 2b) show the image of bilayer hydrogel membrane these pictures show the image scan from -49.9nm to -120.4 nm in height sensor and 90.4pN to -94.8pN in peak force error and the image was taken at 40 nm. For both images we observe that when we have single layer of polymer, we get the smooth surface. while the smoothness decreases when we add another layer.

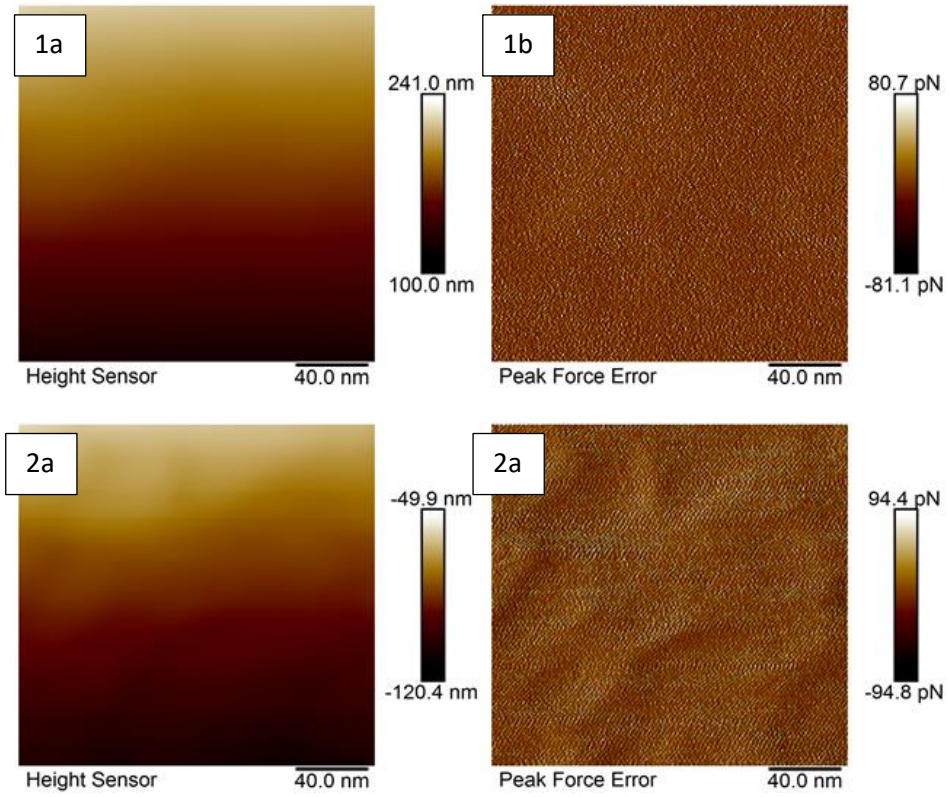

Figure 43 AFM of Pure PVA membrane (1a and 1b) and Bilayer hydrogel membrane (2a and 2b)

fig 45-(1a and 1b) show the image of bilayer hydrogel membrane in which 10 ±5nm size of silver nanoparticles are incorporated these pictures show the image scan from -462.2nm to -802.1nm in height sensor and 89.2pN to -72.7pN in peak force error and the image was taken at 100 nm. fig 45-(2a and 2b) show the image of bilayer hydrogel membrane in which 25 ±5nm size of silver nanoparticles are incorporated these pictures show the image scan from 50nm to -299.8 nm in height sensor and 107.6pN to -108.4pN in peak force error and the image was taken at 100 nm. 45-(3a and 3b) show the image of bilayer hydrogel membrane in which 45 ±5nm size of silver nanoparticles are incorporated these pictures show the image scan from -1.1nm to -59.3 nm in height sensor and 91.9pN to -83.7pN in peak force error and the image was taken at 100 nm. After evaluating these images, we can see that the surface of the bilayer is slightly rougher than PVA, but the surface of the membrane becomes rougher as the size of the nanoparticles increases. When

we incorporate NPs into bilayer membranes, the smoothness of the membranes reduces when we add the larger the size, of NPs and the membrane become the rougher.

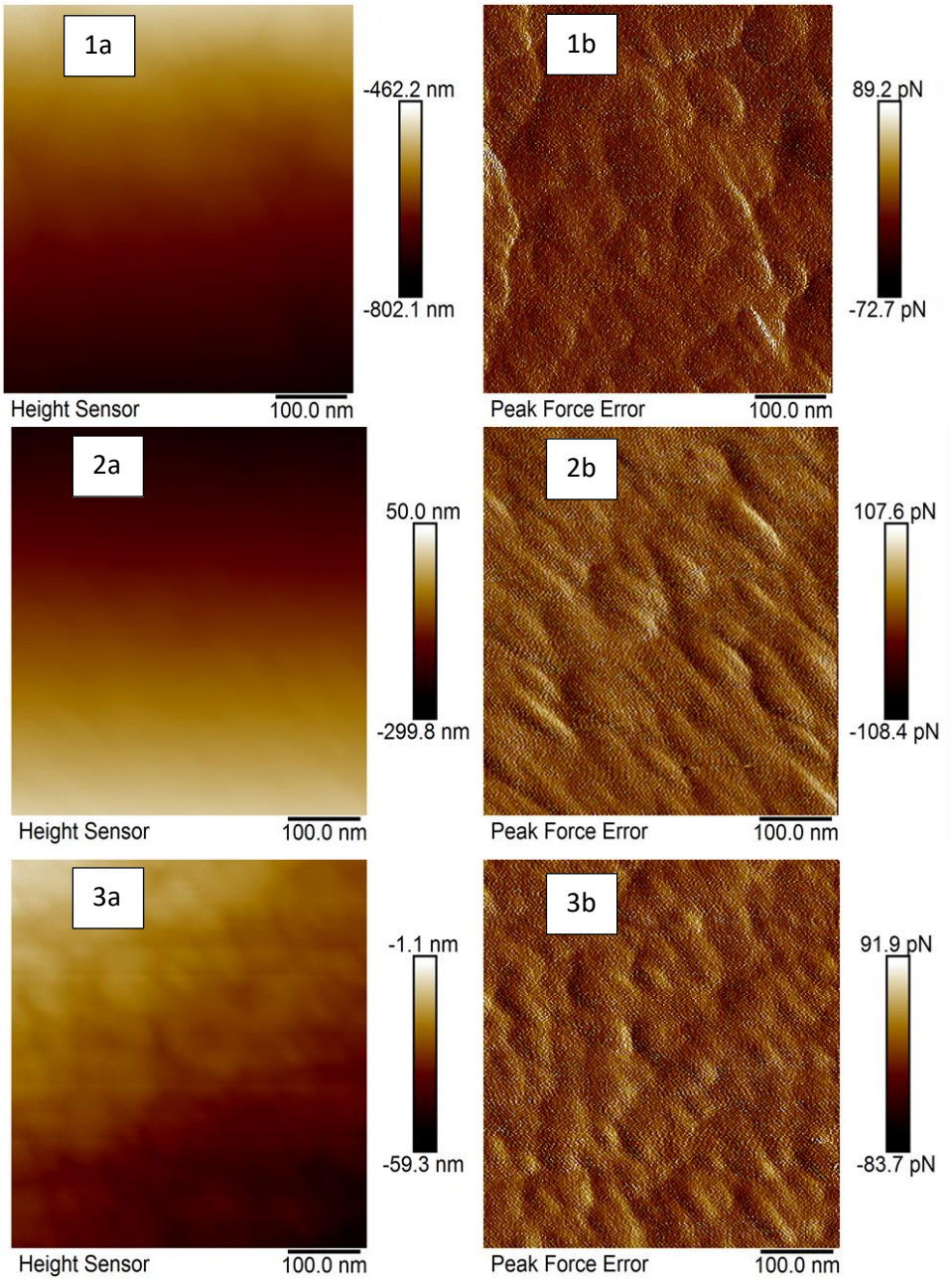

Figure 44 AFM of the incorporated AgNPs of different size (1a and 1b for 10±5nm), (2a and 2b for 25±5nm) and (3a and 3b for 45±5nm)

5.6.4 Thermal Gravimetric analysis (TGA) analysis

Figure 46 illustrate the of curve of TGA of pure PVA, bilayer hydrogel membrane and bilayer hydrogel membrane in which different size of nanoparticles are incorporated. The result demonstrated its unique behavior because these membranes are thermally stable up to 400℃. After that there is change in peak due to degradation of polymers and it is suitable to be applied at normal and even under high temperatures.

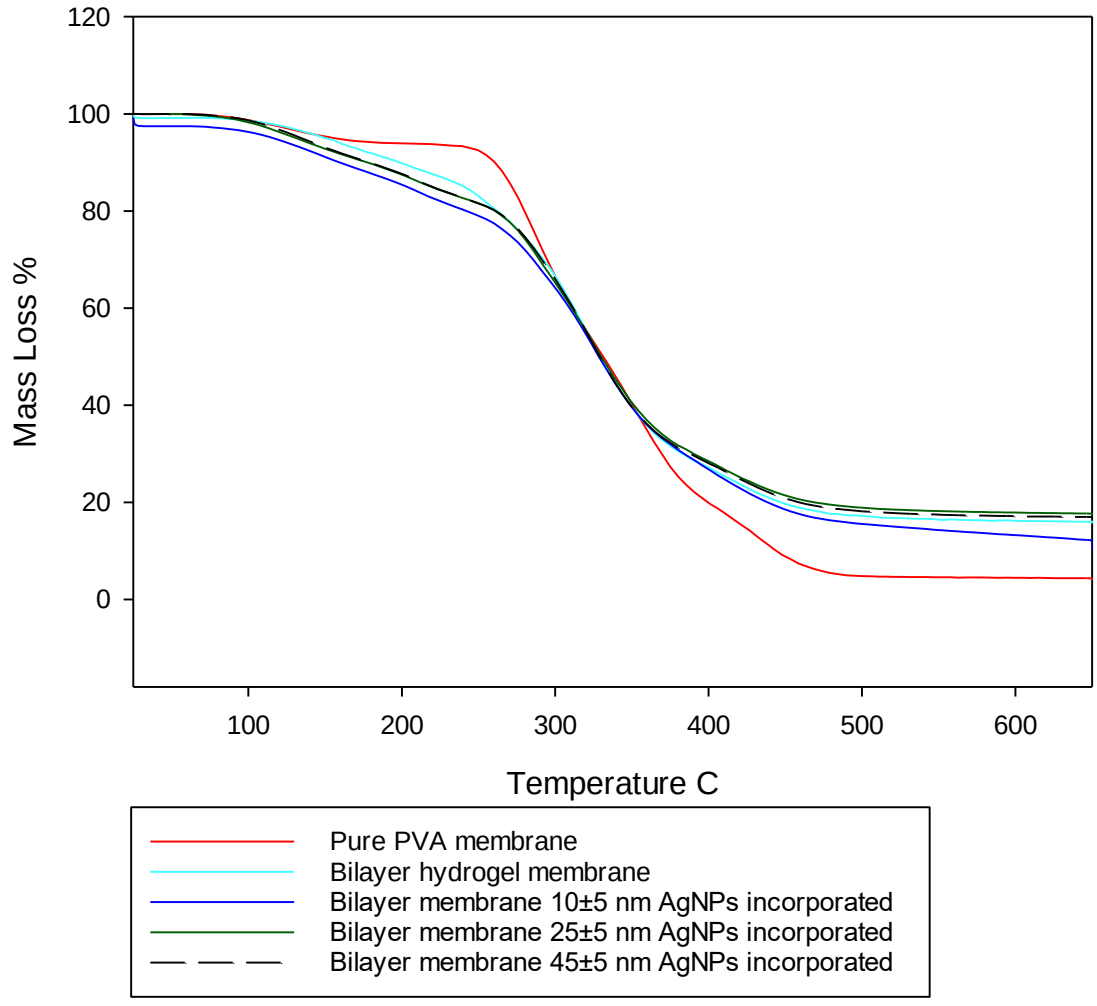

Figure 45 TGA of prepared hydrogel membrane

These TGA curves of PVA, bilayer hydrogel membrane and bilayer hydrogel membrane in which silver nanoparticles are incorporated with different sizes but the shape and

quantity of the silver nanoparticle is constant. After analyzing the TGA graph we observed that there are 3 different regions. The initial weight loss after 70℃ - 250℃ for pure PVA and for bilayer hydrogel membrane and bilayer hydrogel membrane in which nanoparticles are incorporated the initial weight loss at 70℃-180℃ this is due to the amount of solvent that is release or absorb by the polymer and loss of volatile matter. In the second region the degradation of PVA, chitosan, and silver nanoparticles. This is due to dehydration of hydroxyl group and formation of new carbon species; in this stage the functional group of oxygen are removed and from polyene. After that in the third region the degradation of PVA, chitosan and silver nanoparticles occurs when the temperature is above 400℃. After 400℃ the decomposition of PVA chains occurs. After 500℃ - 650℃ carbonization occurs in last stage and in some studies, they have reported shift of degradation from the temperature 250℃ - 350 ℃. So according to result it is confirmed that these bilayer hydrogel membranes are thermally stable up to 200℃.[67]

5.6.5 Moisture Retention capability

The moisture retention capability is a test that is related to the hydrogel properties in which we get the information about the loss of water. Because hydrogel has the ability to absorb huge amounts of water due to its hydrophilic matrix, it is a method in which the hydrogel membrane interacts with the wound surface to check the adsorption capabilities. It keeps the wound moist so that it can recover quickly[50]. We have five different membranes: a blank PVA membrane, a bilayer membrane of PVA/chitosan, and a bilayer membrane of PVA/chitosan with various sizes of AgNPs. However, when we analyze the results, we observe no significant differences in the hydrogel membranes because all the results are in the 80 to 85 %. The introduction of silver nanoparticles of various sizes reduces the moisture retention ability; however, the variation is not significant in comparison to other factors. It provides similar values that are reported for AgNPs. A membrane's excellent moisture retention ability is due to an excess of -OH bonds in the polymeric structure. Water is stuck in the compact structure of the hydrogel membrane due to its hydrophilic nature, and it has no way of escaping from the polymeric network[55]

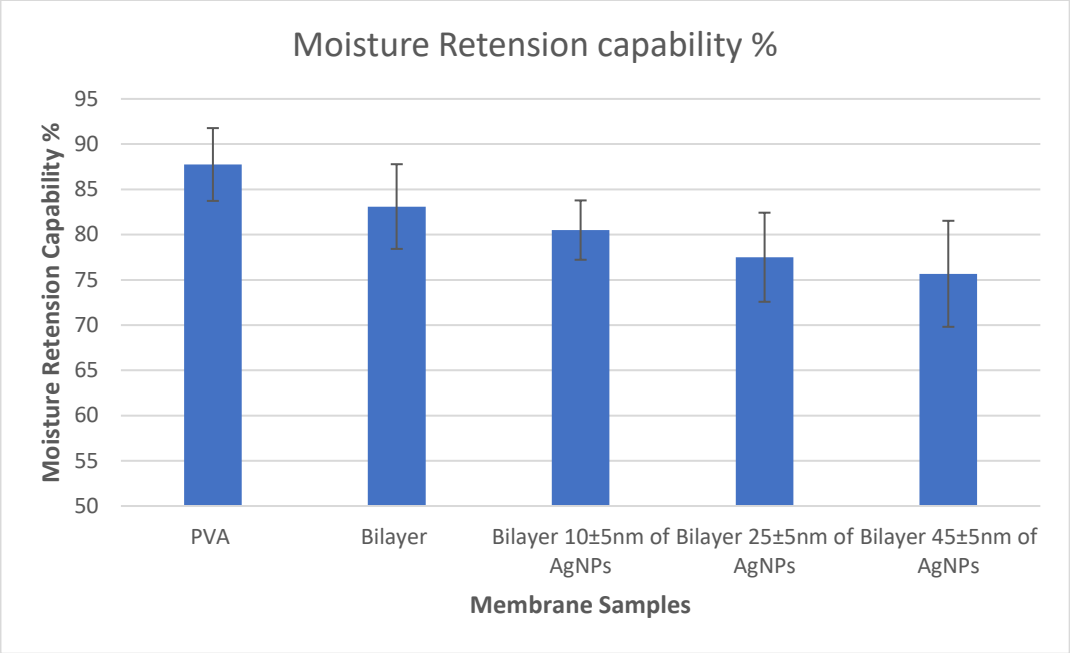

Figure 46 Moisture retention capability % of Prepared membrane sample pure PVA membrane, bilayer membrane, bilayer 10±5nm AgNPs inc, bilayer 25±5nm AgNPs inc and bilayer 45±5nm AgNPs are inc respectively

5.6.6 Water vapor transmission rate (WVTR)

Water vapour transmission rate of the bilayer hydrogel membranes in which in which different size of AgNPs are incorporated are shown in fig 48 different hydrogel membrane are analyzed by WVTR, the hydrogel membrane shows the increasing trends. The negative control is a sealed bottle while on the other hand the positive control is the open bottle. The WVTR for the open bottle is 360.8 $g.m^2.h$ under the given condition. I have been observed that when the membranes were coved, they are greatly reduced in VTR vapour transmission rate. The WVTR for pure PVA membrane, Bilayer hydrogel membrane, bilayer hydrogel membrane in which 10±5nm size particle are incorporated, bilayer hydrogel membrane in which 25±5nm size particles are incorporated and bilayer hydrogel membrane in which 45±5nm size particle are incorporated were 48.10, 60.48, 77.66, 90.41, and 102.0 $g/m^2.h$ respectively. These results are the proof that that these membranes have enough capability to act as barrier in the transmission rate and prevent the water loss from the wound. When we add the NPs in the in the hydrogel membrane structure it helps to enlarge the matrix due to its hydrophilic nature of nanoparticles[68, 69].

These membranes have the ability to reduce water vapour transfer rate because their WVTR values are significantly smaller than an open bottle. Water vapour is transmitted by normal skin at a rate of 8.50g/m^2. h. A damaged skin, on the other hand, can transmit it at a rate of up to 200g/m2. h. The ideal water vapour transfer parameters are 92-190 g/m2 h. As a result, manufactured hydrogels could be used as wound healing materials.

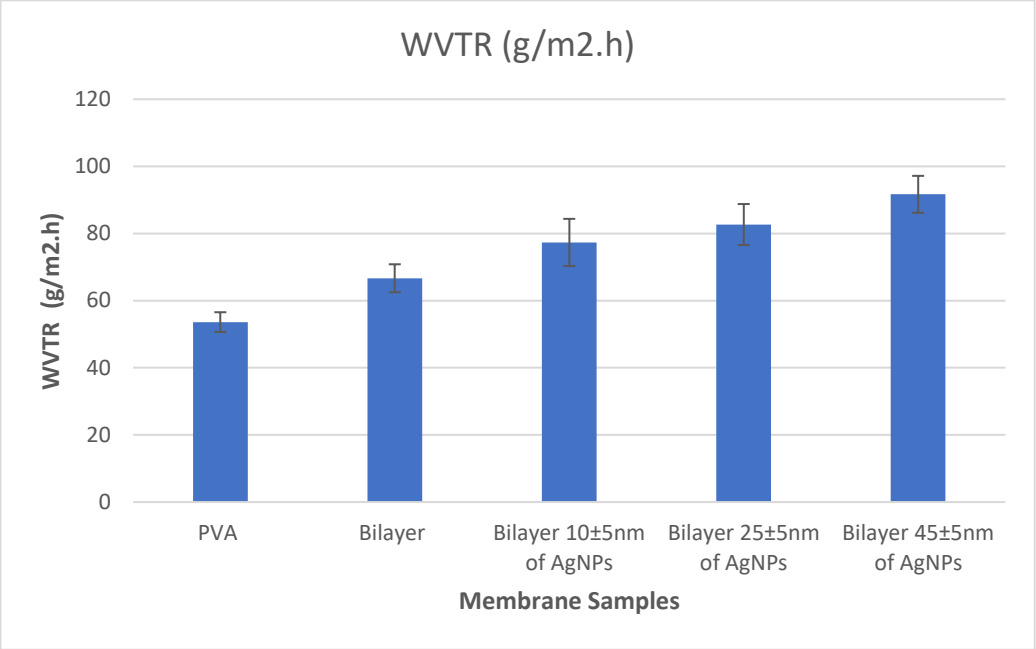

Figure 47 Water Vapour Transmission Rate of prepared hydrogel membrane sample pure PVA membrane, bilayer membrane, bilayer 10±5nm AgNPs inc, bilayer 25±5nm AgNPs inc and bilayer 45±5nm AgNPs are inc respectively

5.6.7 Swelling test

Swelling behaviors of hydrogel is the important parameter when you application is biomedical and pharmaceutical. For wound dressing application the main criteria to fil full is the swelling ability of hydrogel. Wound dressing materials have the ability to absorb wound exudates. When it comes to releasing nanoparticles and using them in a medicine delivery system, the swelling test is crucial. The nature of the polymer, temperature, swelling environment, pH, and degree of crosslinking are factors that influence the swelling ability of hydrogels[61, 70].

For figure 49 we observe that pure PVA membrane show high degree of swelling 70.99 % after that second best is bilayer hydrogel membrane with swelling percent of 67 %. after that there is a $\text{Degree of Swelling}\,(\%) = (W_d - W_s / W_{d)} \times 100$ decline

in the graph if you increase the size of AgNPs in hydrogel membranes. For bilayer hydrogel in which 10±5 nm AgNPs are added, bilayer in which 25±5 nm AgNPs are added and bilayer in which 45±5 nm of AgNPs is added has swelling degree of 63.52%,62.24% and 60.40 % respectively. Degree of swelling % is calculate by using the formula below.

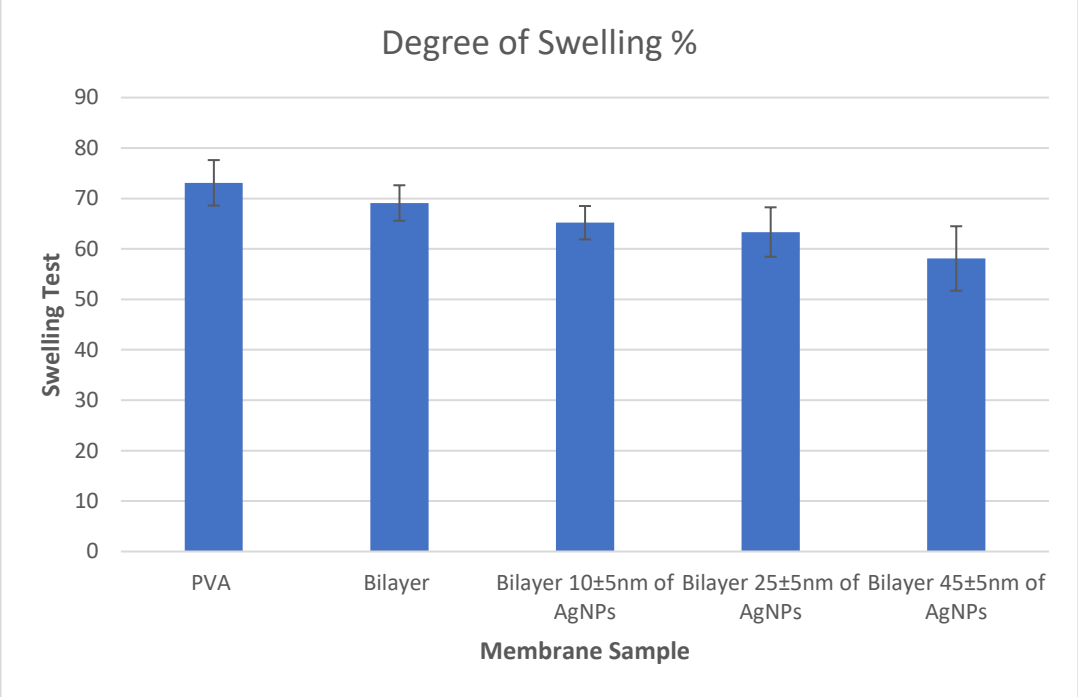

Figure 48 Degree of swelling % of prepared hydrogel membrane sample pure PVA membrane, bilayer membrane, bilayer 10±5nm AgNPs inc, bilayer 25±5nm AgNPs inc and bilayer 45±5nm AgNPs are inc respectively

5.6.8 Antibacterial

Pathogen infection has been a major problem in recent years. Antibiotics are a traditional means of preventing bacterial illnesses. However, bacteria have acquired antibiotic resistance. Furthermore, their large dose necessitates additional treatments and has a higher fatality rate.[71] Ulcers, burns, trauma, and other disorders can cause skin damage and injuries in a variety of ways. A bacterial infection can increase pain and injuries, by putting the patient in more and more danger. Antibiotic resistance is increasingly

posing a threat to frequently used antibiotics. When bacteria are exposed to anti-biotics to destroy them, they develop resistance to the anti-biotics sooner or later. This circumstance causes some people to be concerned. As a result, the manufacturing and development of innovative antibacterial medications, materials, and bandages is critical. The disc diffusion method was used to evaluate the bacterial activity of produced membranes against gram-negative E. coli and Staphylococcus aureus.

The ability of the hydrogel membranes to kill bacteria and preventing their growth is the most important property if they are to be utilized in biomedical particularly wound dressing application. The hydrogel membranes exhibit exceptional antibacterial activity against the microorganisms that are commonly encountered at the wound site. Therefore, the antibacterial nature of prepared polymeric hydrogel membranes was revealed and encouraged its usage as a wound dressing. The results further demonstrated that the hydrogel membranes have the tendency to prevent the wound from infection and accelerate the wound healing process.

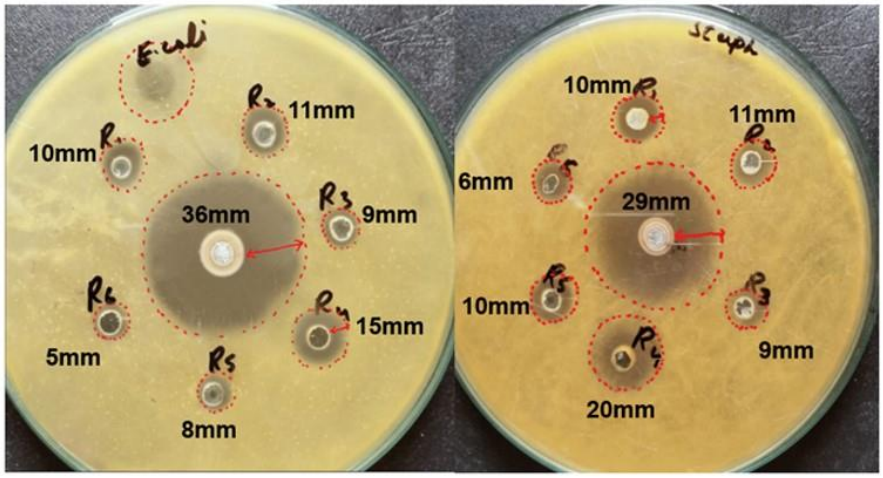

Figure 49 Antibacterial Activity of Hydrogel membranes, R1=Pure PVA, R2=Bilayer Hydrogel Membrane, R3=Bilayer 10±5nm AgNPs, R4=Bilayer 25±5nm AgNPs, R5= Bilayer 45±5nm AgNPs and R6= Controlled without bacteria.

The antibacterial activity of the membranes was determined by using disc diffusion method. Test was performed on two bacteria Staphylococcus and E. coli. The results show that 7 different zone was observed on a petri dish. In E. coli the highest inhibition zone was 15mm for membrane sample, and for positive control the zone was 36mm. but in Staphylococcus the highest inhibition zone was 20mm, and the positive control zone was 29mm. All the sample show antibacterial nature due to presence of chitosan and AgNPs.

5.6.9 Cytotoxicity

MTT assay is used to evaluate the metabolic activity and viability of cells. It is analyzed based on the ability of metabolically active/ live cells to convert water soluble MTT dye [3-(4,5-dimethylthiazol-2-yl)-2,5-diphenyltetrazolium bromide] into an insoluble formazan[62]. The MTT assay helped us to determine the safety profile of hydrogel membranes. The assay revealed that cells treated with all samples and showed high cellular viability. Three different concentration of hydrogel membranes was used one at 100%,70% and 30%. And we observe that if the concentration of membrane is 100%, we get the results between 71% to 82.8%, when the concentration of membrane is 70%, we get the results between 82% to 88.5% and when concentration of membrane is 30%, we get high cell viability between 85% to 92.2%. according to the result we observe that if we increase the nanoparticles size, we get high cell viability percentage. Sample 1= Pure PVA, Sample 2= Bilayer Hydrogel membrane, Sample 3= Bilayer 10±5 nm AgNPs, Sample 4= Bilayer 25±5 nm AgNPs, Sample 5 Bilayer 45±5 nm AgNPs

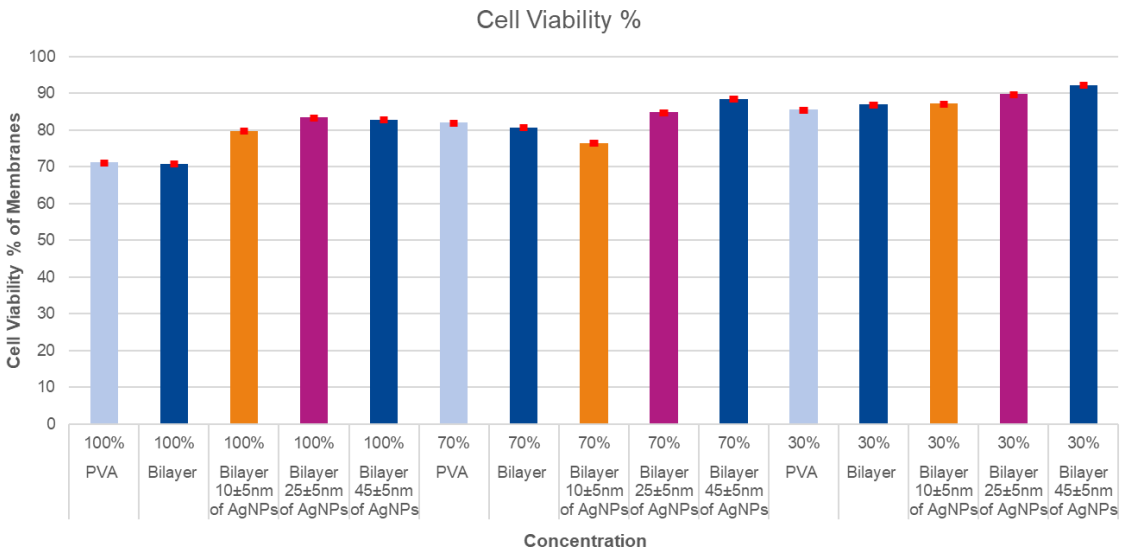

Figure 50 In vitro analysis to evaluate cytotoxicity

Conclusion

In this study silver nanoparticles were successfully prepared by chemical reduction method by using three different reducing agents. We have designed a DOE of 12 experiment on jump software. we modified various parameters like flowrate, concentration of PVP, concentration of AgNO3 and type of reducing agent, we are using two different approaches in first approach we use silver nitrate dropwise and in second approach we use reducing agent dropwise for the synthesis of AgNPs. Bilayer membrane was successfully fabricated by using biodegradable and biocompatible polymer for wound dressing. The main goal of this study is to fabricate the bilayer hydrogel and characterize that bilayer. To give antibacterial nature we play with the sizes of silver nanoparticle while the shape and quantity of silver nanoparticle in membranes is constant. The AgNPs were characterize by S(T)EM, SEM Apreo, FTIR, XRD, Zetasizer and UV Vis to evaluate the crystallinity, surface morphology, Hydrodynamic size, LSPR peak and functional group. The S(T)EM and SEM Apreo confirm the morphology of AgNPs, XRD confirm the fabrication of silver nanoparticles and FTIR strong bell shape absorption band at $1663cm^{-1}$ these band are form due to carbonyl group due to stretching vibration of **C = O** this caused by the presence of PVP. The LSPR peak of silver nanoparticle was found in the range of 390 to 410nm. After fabrication of AgNPs we incorporated different sizes of AgNPs in bilayer hydrogel membrane the SEM Apreo confirm the formation of bilayer, AFM dimension icon show the surface morphology and roughness on the membranes, XRD confirm the presence of AgNPs in membranes. To check the thermal stability TGA was done. Some physical parameters like swelling test, moisture retention and water vapor transmission rate were also done. The antibacterial activity of the bilayer membranes was done by using disc diffusion method, the reported result show promising numbers apart from its antibacterial activity AgNPs also participate in the strengthening of bilayer hydrogel membrane. MTT assay test was conducted to see cell viability % and we observe that at low concentration we get the best results between 85% to 92.2%.

References

[1]. Tavakoli, J., S. Mirzaei, and Y. Tang, *Cost-effective double-layer hydrogel composites for wound dressing applications.* Polymers, 2018. **10**(3): p. 305.

[2]. Zeng, D., S. Shen, and D. Fan, *Molecular design, synthesis strategies and recent advances of hydrogels for wound dressing applications.* Chinese Journal of Chemical Engineering, 2021. **30**: p. 308-320.

[3]. Darwin, E. and M. Tomic-Canic, *Healing chronic wounds: current challenges and potential solutions.* Current dermatology reports, 2018. **7**(4): p. 296-302.

[4]. Priya, S.G., et al., *Bilayer cryogel wound dressing and skin regeneration grafts for the treatment of acute skin wounds.* ACS applied materials & interfaces, 2016. **8**(24): p. 15145-15159.

[5]. Feynman, R.P.J.C.I.o.T., *There's plenty of room at the bottom.* Engineering Science magazine, 1960.

[6]. Laurent, S., et al., *Magnetic iron oxide nanoparticles: synthesis, stabilization, vectorization, physicochemical characterizations, and biological applications.* Chemical reviews, 2008. **108**(6): p. 2064-2110.

[7]. Tiwari, J.N., R.N. Tiwari, and K.S. Kim, *Zero-dimensional, one-dimensional, two-dimensional and three-dimensional nanostructured materials for advanced electrochemical energy devices.* Progress in Materials Science, 2012. **57**(4): p. 724-803.

[8]. Li, N., P. Zhao, and D. Astruc, *Anisotropic gold nanoparticles: synthesis, properties, applications, and toxicity.* Angewandte Chemie International Edition, 2014. **53**(7): p. 1756-1789.

[9]. Taylor, M.G., et al., *Catalyst design based on morphology-and environment-dependent adsorption on metal nanoparticles.* ACS Catalysis, 2015. **5**(11): p. 6296-6301.

[10]. Astefanei, A., O. Núñez, and M.T. Galceran, *Characterisation and determination of fullerenes: a critical review.* Analytica chimica acta, 2015. **882**: p. 1-21.

[11]. Elliott, J.A., et al., *Atomistic modelling of CVD synthesis of carbon nanotubes and graphene.* Nanoscale, 2013. **5**(15): p. 6662-6676.

[12]. Dreaden, E.C., et al., *The golden age: gold nanoparticles for biomedicine.* Chemical Society Reviews, 2012. **41**(7): p. 2740-2779.

[13]. Sigmund, W., et al., *Processing and structure relationships in electrospinning of ceramic fiber systems.* Journal of the American Ceramic Society, 2006. **89**(2): p. 395-407.

[14]. Mansha, M., et al., *Synthesis, characterization and visible-light-driven photoelectrochemical hydrogen evolution reaction of carbazole-containing conjugated polymers.* International Journal of Hydrogen Energy, 2017. **42**(16): p. 10952-10961.

[15]. Rao, J.P. and K.E. Geckeler, *Polymer nanoparticles: preparation techniques and size-control parameters.* Progress in polymer science, 2011. **36**(7): p. 887-913.

[16]. Gutierrez, R.M.P., J.V.M. Mendez, and I.A. Vazquez, *A novel approach to the oral delivery of bionanostructures for systemic disease,* in *Nanostructures for Oral Medicine*. 2017, Elsevier. p. 27-59.

[17]. Sajanlal, P.R., et al., *Anisotropic nanomaterials: structure, growth, assembly, and functions.* Nano reviews, 2011. **2**(1): p. 5883.

[18]. Von Nussbaum, F., et al., *Antibacterial natural products in medicinal chemistry—exodus or revival?* Angewandte Chemie International Edition, 2006. **45**(31): p. 5072-5129.

[19]. Mørk, T., et al., *Comparison of Staphylococcus aureus genotypes recovered from cases of bovine, ovine, and caprine mastitis.* Journal of clinical microbiology, 2005. **43**(8): p. 3979-3984.

[20]. Baker-Austin, C., et al., *Major uncertainties and future research opportunities in metal–antibiotic co-selection.* Trends in Microbiology, 2006. **4**(14): p. 176-182.

[21]. Huh, A.J. and Y.J. Kwon, *"Nanoantibiotics": a new paradigm for treating infectious diseases using nanomaterials in the antibiotics resistant era.* Journal of controlled release, 2011. **156**(2): p. 128-145.

[22]. Xia, Y., *Nanomaterials at work in biomedical research.* Nature materials, 2008. **7**(10): p. 758-760.

[23]. Chatterjee, A.K., R. Chakraborty, and T. Basu, *Mechanism of antibacterial activity of copper nanoparticles.* Nanotechnology, 2014. **25**(13): p. 135101.

[24]. Rigo, C., et al., *Active silver nanoparticles for wound healing.* International journal of molecular sciences, 2013. **14**(3): p. 4817-4840.

[25]. Huang, H. and Y. Yang, *Preparation of silver nanoparticles in inorganic clay suspensions.* Composites Science and Technology, 2008. **68**(14): p. 2948-2953.

[26]. Zhang, X.-F., *Zhi-Guo liu, Wei shen, Sangiliyandi Gurunathan. SilverNanoparticles: Synthesis, Characterization, Properties, Applications, and Therapeutic Approaches.* International Journal of Molecular Sciences, 2016. **17**: p. 1534.

[27]. Iacono, S.T. and A.R. Jennings, *Recent studies on fluorinated silica nanometer-sized particles.* Nanomaterials, 2019. **9**(5): p. 684.

[28]. Chen, S.-F. and H. Zhang, *Aggregation kinetics of nanosilver in different water conditions.* Advances in natural sciences: nanoscience and nanotechnology, 2012. **3**(3): p. 035006.

[29]. Shanmugam, N., et al., *Biosynthesis of silver nanoparticles from the marine seaweed Sargassum wightii and their antibacterial activity against some human pathogens.* Applied Nanoscience, 2014. **4**(7): p. 881-888.

[30]. Petryayeva, E. and U.J. Krull, *Localized surface plasmon resonance: Nanostructures, bioassays and biosensing—A review.* Analytica chimica acta, 2011. **706**(1): p. 8-24.

[31]. Kwizera, E.A., et al., *Synthesis and properties of magnetic-optical core–shell nanoparticles.* RSC advances, 2017. **7**(28): p. 17137-17153.

[32]. Bandyopadhyay, S., *Fabrication and Applications of Nanomaterials.* McGraw-Hill, 2019.

[33]. Hadilou, N., et al., *An optimal architecture of magneto-plasmonic core–shell nanoparticles for potential photothermal applications.* Physical Chemistry Chemical Physics, 2020. **22**(25): p. 14318-14328.

[34]. Kim, M., J.H. Lee, and J.M. Nam, *Plasmonic photothermal nanoparticles for biomedical applications.* Advanced Science, 2019. **6**(17): p. 1900471.

[35]. Riley, R.S. and E.S. Day, *Gold nanoparticle-mediated photothermal therapy: applications and opportunities for multimodal cancer treatment.* Wiley

Interdisciplinary Reviews: Nanomedicine and Nanobiotechnology, 2017. **9**(4): p. e1449.

[36]. Bhatia, P., S. Verma, and M. Sinha, *Optical properties simulation of magneto-plasmonic alloys nanostructures.* Plasmonics, 2019. **14**(3): p. 611-622.

[37]. Okolieocha, C., et al., *Microcellular to nanocellular polymer foams: Progress (2004–2015) and future directions–A review.* European Polymer Journal, 2015. **73**: p. 500-519.

[38]. Thanh, N.T., N. Maclean, and S. Mahiddine, *Mechanisms of nucleation and growth of nanoparticles in solution.* Chemical reviews, 2014. **114**(15): p. 7610-7630.

[39]. Polte, J., *Fundamental growth principles of colloidal metal nanoparticles–a new perspective.* CrystEngComm, 2015. **17**(36): p. 6809-6830.

[40]. Ding, B., et al., *Material nucleation/growth competition tuning towards highly reproducible planar perovskite solar cells with efficiency exceeding 20%*. Journal of Materials Chemistry A, 2017. **5**(15): p. 6840-6848.

[41]. Mer, V.K.L., *Nucleation in Phase Transitions.* Industrial & Engineering Chemistry, 1952. **44**(6): p. 1270-1277.

[42]. Simões, D., et al., *Recent advances on antimicrobial wound dressing: A review.* European Journal of Pharmaceutics and Biopharmaceutics, 2018. **127**: p. 130-141.

[43]. Hu, H. and F.-J. Xu, *Rational design and latest advances of polysaccharide-based hydrogels for wound healing.* Biomaterials science, 2020. **8**(8): p. 2084-2101.

[44]. Kamoun, E.A., E.-R.S. Kenawy, and X. Chen, *A review on polymeric hydrogel membranes for wound dressing applications: PVA-based hydrogel dressings.* Journal of advanced research, 2017. **8**(3): p. 217-233.

[45]. Ahmed, E.M., *Hydrogel: Preparation, characterization, and applications: A review.* Journal of advanced research, 2015. **6**(2): p. 105-121.

[46]. Gurtner, G.C., et al., *Wound repair and regeneration.* Nature, 2008. **453**(7193): p. 314-321.

[47]. Tiwari, V., *Burn wound: how it differs from other wounds?* Indian journal of plastic surgery, 2012. **45**(02): p. 364-373.

[48]. Hosgood, G., *Stages of wound healing and their clinical relevance.* Veterinary Clinics: Small Animal Practice, 2006. **36**(4): p. 667-685.

[49]. Ho, J., et al., *Current advancements and strategies in tissue engineering for wound healing: a comprehensive review.* Advances in wound care, 2017. **6**(6): p. 191-209.

[50]. Fan, Z., et al., *A novel wound dressing based on Ag/graphene polymer hydrogel: effectively kill bacteria and accelerate wound healing.* Advanced Functional Materials, 2014. **24**(25): p. 3933-3943.

[51]. Kalashnikova, I., S. Das, and S. Seal, *Nanomaterials for wound healing: scope and advancement.* Nanomedicine, 2015. **10**(16): p. 2593-2612.

[52]. Wells, A., A. Nuschke, and C.C. Yates, *Skin tissue repair: Matrix microenvironmental influences.* Matrix Biology, 2016. **49**: p. 25-36.

[53]. Axibal, E. and M. Brown, *Surgical dressings and novel skin substitutes.* Dermatologic clinics, 2019. **37**(3): p. 349-366.

[54]. Rahimi, M., et al., *A novel bioactive quaternized chitosan and its silver-containing nanocomposites as a potent antimicrobial wound dressing: Structural and biological properties.* Materials Science and Engineering: C, 2019. **101**: p. 360-369.

[55]. Ye, H., J. Cheng, and K. Yu, *In situ reduction of silver nanoparticles by gelatin to obtain porous silver nanoparticle/chitosan composites with enhanced antimicrobial and wound-healing activity.* International journal of biological macromolecules, 2019. **121**: p. 633-642.

[56]. Ellis-Behnke, R.G., et al., *Nano hemostat solution: immediate hemostasis at the nanoscale.* Nanomedicine: Nanotechnology, Biology and Medicine, 2006. **2**(4): p. 207-215.

[57]. Kohli, R., *Methods for monitoring and measuring cleanliness of surfaces,* in *Developments in Surface Contamination and Cleaning*. 2012, Elsevier. p. 107-178.

[58]. Ramachandran, V.S. and J.J. Beaudoin, *Handbook of analytical techniques in concrete science and technology: principles, techniques and applications*. 2000: Elsevier.

[59]. Roy, N., et al., *Effectiveness of polymer sheet layer to protect hydrogel dressings.* Trends in Colloid and Interface Science XXIV, 2011: p. 127-130.

[60]. Farzinfar, E. and A. Paydayesh, *Investigation of polyvinyl alcohol nanocomposite hydrogels containing chitosan nanoparticles as wound dressing.* International Journal of Polymeric Materials and Polymeric Biomaterials, 2019. **68**(11): p. 628-638.

[61]. Khorasani, M.T., et al., *Incorporation of ZnO nanoparticles into heparinised polyvinyl alcohol/chitosan hydrogels for wound dressing application.* International journal of biological macromolecules, 2018. **114**: p. 1203-1215.

[62]. Abud, M.B., et al., *In vivo and in vitro toxicity evaluation of liposome-encapsulated sirolimus.* International Journal of Retina and Vitreous, 2019. **5**(1): p. 1-10.

[63]. Tang, S., et al., *PVP-assisted sonoelectrochemical growth of silver nanostructures with various shapes.* Materials Chemistry and Physics, 2009. **116**(2-3): p. 464-468.

[64]. Jana, D. and G. De, *Spontaneous generation and shape conversion of silver nanoparticles in alumina sol, and shaped silver nanoparticle incorporated alumina films.* Journal of Materials Chemistry, 2011. **21**(16): p. 6072-6078.

[65]. Seoudi, R., A. Fouda, and D. Elmenshawy, *Synthesis, characterization and vibrational spectroscopic studies of different particle size of gold nanoparticle capped with polyvinylpyrrolidone.* Physica B: Condensed Matter, 2010. **405**(3): p. 906-911.

[66]. Kayaci, F. and T. Uyar, *Solid inclusion complexes of vanillin with cyclodextrins: their formation, characterization, and high-temperature stability.* Journal of agricultural and food chemistry, 2011. **59**(21): p. 11772-11778.

[67]. Tanpichai, S. and K. Oksman, *Cross-linked nanocomposite hydrogels based on cellulose nanocrystals and PVA: Mechanical properties and creep recovery.* Composites Part A: Applied Science and Manufacturing, 2016. **88**: p. 226-233.

[68]. Huang, Y., et al., *Protonated g-C3N4/Ti3+ self-doped TiO2 nanocomposite films: Room-temperature preparation, hydrophilicity, and application for photocatalytic NOx removal.* Applied Catalysis B: Environmental, 2019. **240**: p. 122-131.

[69]. Zhang, M., et al., *Ag@ MOF-loaded chitosan nanoparticle and polyvinyl alcohol/sodium alginate/chitosan bilayer dressing for wound healing applications.* International Journal of Biological Macromolecules, 2021. **175**: p. 481-494.

[70]. Kim, S.W., Y.H. Bae, and T. Okano, *Hydrogels: swelling, drug loading, and release.* Pharmaceutical research, 1992. **9**(3): p. 283-290.

[71]. Riley, M.A., et al., *Resistance is futile: the bacteriocin model for addressing the antibiotic resistance challenge*. 2012, Portland Press Ltd.